Inorganic Chemistry

Article

pubs.acs.org/IC

Near-IR Broadband-Absorbing *trans*-Bisphosphine Pt(II) Bisacetylide Complexes: Preparation and Study of the Photophysics

Wenbo Yang,[†] Ahmet Karatay,[‡] Jianzhang Zhao,*[,†] Jian Song,[§] Liang Zhao,[†] Yongheng Xing,*[,§] Caishun Zhang,[†] Cheng He,[†] Halime Gul Yaglioglu,[‡] Mustafa Hayvali,*[,∥] Ayhan Elmali,[‡] and Betül Küçüköz[‡]

[†]State Key Laboratory of Fine Chemicals, School of Chemical Engineering, Dalian University of Technology, E-208 West Campus, 2 Ling Gong Rd., Dalian 116024, P. R. China

[‡]Department of Engineering Physics, Faculty of Engineering and [∥]Department of Chemistry, Faculty of Science, Ankara University, 06100 Beşevler, Ankara, Turkey

[§]College of Chemistry and Chemical Engineering, Liaoning Normal University, Dalian 116029, P. R. China

Supporting Information

ABSTRACT: Broadband near-IR absorbing *trans*-bis(trialkylphosphine) Pt(II) bisacetylide binuclear complex (**Pt−1**) was prepared with boron-dipyrromethene (Bodipy) and styrylBodipy acetylide ligands. **Pt−1** shows strong absorption bands at 731 and 503 nm. Singlet energy transfer (EnT) and efficient intersystem crossing of the central coordinated Bodipy ligand were proposed to be responsible for the efficient funneling of the excitation energy to the triplet-state manifold. Reference complexes containing only a single Bodipy ligand were prepared for comparison (with styrylBodipy ligand **Pt−0** or Bodipy ligand **Pt−2**). The molecular structures were confirmed by single-crystal X-ray diffraction. The photophysical properties were studied with steady-state and time-resolved transient absorption spectroscopies, electrochemical characterization, and density functional theory/time-dependent density functional theory calculations. Dual fluorescence was observed for **Pt−1**. Singlet EnT in **Pt−1** was proposed based on the fluorescence quenching/excitation spectra, and femtosecond transient absorption spectra (energy transfer rate constant k_{EnT} = 2.2 × 10^{10} s^{-1}). With nanosecond transient absorption spectra, intramolecular *triplet*-state energy transfer in **Pt−1** was proved. Gibbs free energy changes of charge separation indicate that the photoinduced intramolecular electron transfer in **Pt−1** is thermodynamically prohibited. Intermolecular triplet transfer between **Pt−2** and **L−1** was studied with nanosecond transient absorption spectra; the EnT rate and energy transfer efficiency were determined as 3.6 × 10^4 s^{-1} and 94.5%, respectively. The singlet oxygen ($^1O_2$) photosensitizing of **Pt−1** was improved as compared to the complexes containing only a single visible-light-absorbing chromophore.

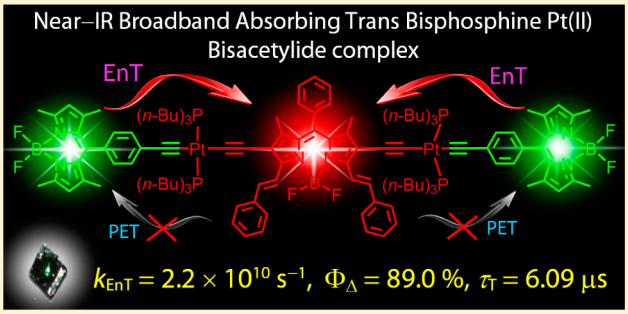

INTRODUCTION

Transition metal complexes, such as Pt(II) complexes, have attracted much attention due to the applications in photocatalysis,[1−3] hydrogen (H_2) production,[4,5] photoredox catalytic organic reactions,[6,7] electroluminescence and luminescence bioimaging,[8−11] molecular sensors and devices,[12,13] photodynamic therapy,[14,15] and more recently in triplet−triplet annihilation (TTA) upconversion.[16−19] Concerning most of these applications, the complexes play the pivotal role via photoinduced *intermolecular* energy transfer (EnT) or electron transfer (ET).[19] Thus, the visible-light-harvesting ability and the lifetime of the triplet excited state of the complexes are the two crucial parameters for the transition metal complexes to be used as triplet photosensitizers, because the intermolecular EnT and ET can be enhanced by the strong light absorption (a prerequisite for formation of abundant photosensitizers at excited states) and the long-lived triplet excited states.[19]

In this context, the conventional Pt(II) complexes are suffering from some limitations.[1] First, the complexes usually show very weak absorption in visible spectral region, and the absorption is usually in UV or blue range of the spectrum.[20−26] Very few complexes show absorption in visible spectra range.[27−30] Second, the lifetime of the triplet excited state is usually short, less than 10 μs.[1] Third, the molecular structure profile of the complexes is based on a single visible-light-harvesting chromophore; thus, there is only one major absorption band in visible spectral range for these complexes. As a result, harvesting of the excitation energy of a broadband light source, such as solar light, is inefficient.[1,19]

To address the above challenges, recently we prepared a series of Pt(II),[28,29,31−33] Ru(II),[34,35] Ir(III),[36−39] and Re(I)

Received: May 16, 2015
Published: July 21, 2015

DOI: 10.1021/acs.inorgchem.5b01107
Inorg. Chem. 2015, 54, 7492−7505

Scheme 1. Preparation of the Complexes Pt−0 and Pt−1[a]

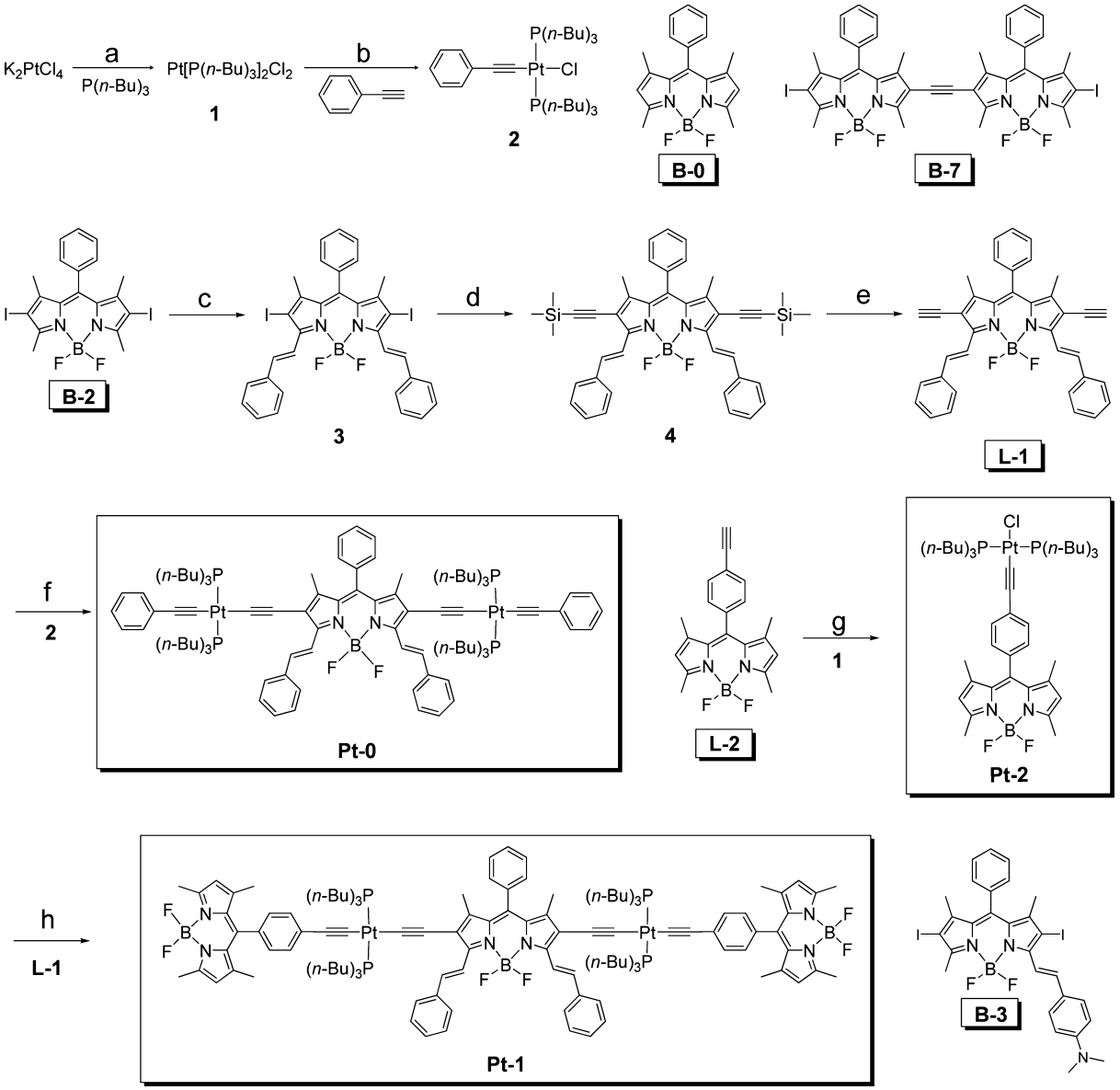

[a]The molecular structures of the ligands and reference complexes are also shown. (a) Deionized water, Ar, RT, 3 h, yield 57.7%. (b) Dried $NHEt_2$, Ar, 45 °C, 8 h, yield: 79.8%. (c) Benzaldehyde, acetic acid, piperidine, Ar, microwave irradiation 150 °C, 6 min, yield: 85.1%. (d) Trimethylsilylacetylene, $Pd(PPh_3)_2Cl_2$, PPh_3, CuI, distilled THF, $(^iPr)_2NH$, Ar, 68 °C, 6 h, yield: 77.0%. (e) $Bu_4NF{\cdot}3H_2O$, distilled THF, Ar, −78 °C, 0.5 h, yield: 58.4%. (f) CuI, distilled THF, dried $NHEt_2$, Ar, RT, 0.5 h, yield: 61.9%. (g) CuI, distilled THF, dried $NHET_2$, Ar, RT, 3 h, yield 43.0%. (h) Dried $NHEt_2$, Ar, 45 °C, 9 h, yield: 33.4%.

complexes,[40,41] using organic chromophores of boron dipyrromethene (Bodipy), naphthaleneimide, naphthalenediimide, perylenediimide, rhodamine, and fluorescein.[19,42] Strong absorption of visible light and long-lived intraligand triplet state (^{3}IL) was observed for these complexes. These complexes have been used for photocatalysis and TTA upconversion.[17,19,42] We also prepared Pt(II) complexes that contain two different visible-light-absorbing chromophores; thus, broadband visible-light-absorption was observed.[30,43] However, there is still much room left to fully explore the molecular structural diversity of this kind of complex; for example, the absorption wavelength of these complexes are usually shorter than 600 nm. This short absorption wavelength is detrimental for luminescence bioimaging in vivo or photodynamic therapy (PDT), for which near-IR absorption/emission is desired.[30,43] Second, the limited examples of the broadband absorbing complexes show only the energy acceptor's emission. Dual emission is rare for Pt(II) complexes.[9,44,45]

To address these limitations, herein we prepared near-IR broadband absorbing binuclear *trans*-bis(tributylphosphine) Pt(II) bisacetylide complex, which contains two types of different Bodipy ligands (Bodipy and styrylBodipy. **Pt−1**. Scheme 1). Bodipy was selected as the light-harvesting antenna due to its strong absorption of visible light, high fluorescence quantum yields (inhibited non-radiative decay), good photostability, and feasible derivatization.[46−52] The central coordinated styrylBodipy in **Pt−1** is with larger π-conjugation framework than the peripheral coordinated Bodipy ligands (Scheme 1). The central coordinated styrylBodipy section shows absorption/emission in the near-IR region (660−800

DOI: 10.1021/acs.inorgchem.5b01107
Inorg. Chem. 2015, 54, 7492−7505

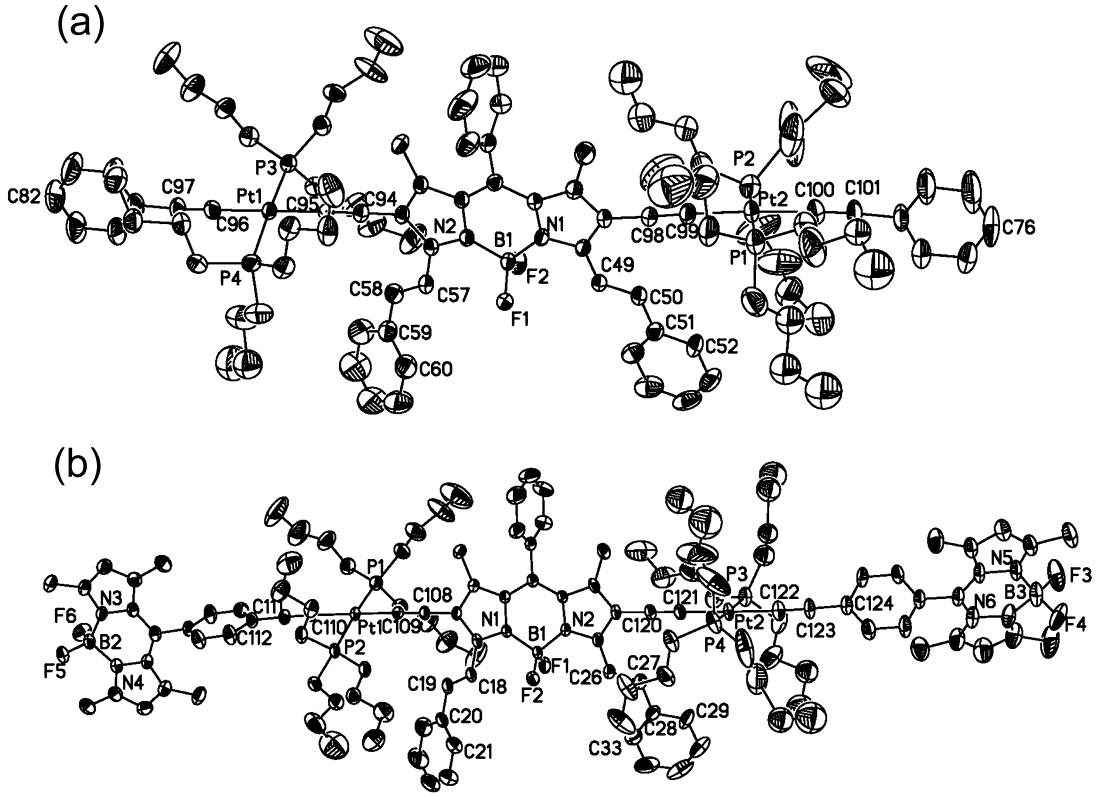

Figure 1. ORTEP view of the single-crystal structure of (a) **Pt−0** and (b) **Pt−1** with 30% thermal ellipsoids.

nm), and the peripheral coordinated Bodipy ligands give strong absorption at 500 nm. The photophysical properties of the complexes were studied with steady-state and time-resolved transient spectroscopy. Ultrafast singlet-energy transfer via the through-bond energy-transfer (TBET) mechanism was proposed for the broadband visible-light-absorbing complex, because the spectral overlap integral is too small to ensure a fast fluorescence-resonance energy-transfer (FRET) EnT process (Förster mechanism). Dual emission was observed, which is unprecedented for *trans*-bisphosphine Pt(II) bisacetylide complexes. The complex shows efficient singlet oxygen ($^1O_2$) photosensitizing ability (Φ_Δ = 89.0%). Intramolecular and intermolecular triplet-energy transfers were studied with nanosecond time-resolved transient absorption spectroscopy.

RESULTS AND DISCUSSION

Design and Synthesis of the Complexes. *trans*-Bis(trialkylphosphine) Pt(II) bisacetylide complexes are of particular interest because it is feasible to introduce heteroleptic (different) visible-light-absorbing ligands into the molecules, simply by using different acetylide ligands.[53−55] Recently we prepared N^N Pt(II) bisacetylide complex with heteroleptic acetylide ligands.[56] But two different acetylide ligands are unable to be introduced in a stepwise way. Previously unmodified Bodipy ligands were used for preparation of the Pt(II) complexes, but the absorption wavelength is shorter than 600 nm.[28,30,43] Herein we used styrylBodipy as an acetylide ligand, which shows absorption at 648 nm. Upon coordination with Pt(II), the absorption is shifted to 731 nm, that is, in the near-IR region. To the best of our knowledge, no *trans*-bis(trialkylphosphine) Pt(II) bisacetylide complexes have been reported showing absorption in near-IR spectral region.[53−55,57]

The attachment of ethynyl moieties to Bodipy is via Sonogashira coupling reactions (Scheme 1).[38,58] StyrylBodipy ligand **L−1** was obtained by the condensation of Bodipy with benzaldehyde.[50] **Pt−1** was prepared with **Pt−2** and **L−1** as the starting materials. All the compounds were obtained in moderate-to-satisfactory yields. The molecular structures were fully verified with ^{1}H NMR, ^{13}C NMR, and high-resolution mass spectrometry (HRMS).

Single-Crystal Molecular Structures. The molecular structures of **Pt−0** and **Pt−1** were determined by single-crystal X-ray diffraction (Figure 1 and Table 1).[59] For **Pt−0**, the two Pt(II) coordination centers take planar square geometries. For example, the bond angle of C(96)−Pt(1)−P(3) is 91.22(13)°, the bond angle of C(95)−Pt(1)−C(96) is 178.79(18)°, and the P(3)−Pt(1)−P(4) bond angle is 176.84(4)°. A similar result was observed for the Pt(2) coordination center. These values are close to a previously reported *trans*-bis(trialkylphosphine) Pt(II) bisacetylide complex.[53] The Pt(1)−C(95) bond length is 1.992(4) Å, which is close to the previously reported values (1.981−2.015 Å).[53] The C≡C bond lengths are in the range of 1.193−1.209 Å, which is close to the literature values (1.192−1.233 Å).[59]

For the coordinated styrylBodipy, the two styryl moiety planes twisted toward the π-core of the Bodipy chromophore, presumably due to the steric hindrance exerted by the two Pt(II) coordination centers and the phosphine ligands. For example, the dihedral angles of C(49)−C(50)−C(51)−C(52) and C(57)−C(58)−C(59)−C(60) were observed as 12.611° and 22.140°, respectively. Previously in an uncoordinated styrylBodipy molecule, the dihedral angles of the two styryl moieties with the π-core of the Bodipy chromophore are much smaller.[60] **Pt−0** shows a rodlike long molecule axial of 30.6527 Å (the distance of C(76) to C(82)), with the C−Pt−C bond

DOI: 10.1021/acs.inorgchem.5b01107
Inorg. Chem. 2015, 54, 7492−7505

Table 1. Crystallographic Data for Pt−0 and Pt−1

complexes	**Pt−0**	**Pt−1**
sum formula	$C_{101}H_{143}BF_2N_2P_4Pt_2$	$C_{127}H_{169}B_3F_6N_6P_4Pt_2$
M (g mol^{-1})	1948.04	2440.17
temperature/K	296(2)	296(2)
crystal system	monoclinic	triclinic
space group	$P2_1/n$	$P\bar{1}$
a (Å)	21.7912(18)	15.292(3)
b (Å)	14.8974(12)	17.398(3)
c (Å)	33.153(3)	25.540(4)
α (deg)	90.00	102.092(3)
β (deg)	108.1610(10)	94.011(3)
γ (deg)	90.00	103.690(3)
volume/Å^3	10 226.4(14)	6403.9(19)
Z	4	2
D_{calc}/g·cm^{-3}	1.265	1.265
crystal size (mm)	0.34 × 0.28 × 0.26	0.35 × 0.27 × 0.15
F (000)	4008	2516
μ (Mo Kα)/mm^{-1}	2.841	2.288
θ (deg)	1.88−28.27	1.52−28.41
reflections collected	62 775	47 943
independent reflections	24 775	31 660
parameters	1239	1526
largest diff. peak and hole (e Å^{-3})	0.822, −0.543	1.358, −0.721
goodness of fit	1.012	1.014
R^a	0.0477[b]	0.0496[b]
$\omega R_2{}^a$	0.0823[b]	0.1113[b]

[a] $R = \sum||F_o| - |F_c||/\sum|F_o|$, $wR_2 = [\sum(w(F_o^2 - F_c^2)^2)/\sum(w(F_o^2)^2)]1/2$; $[F_o > 4\sigma(F_o)]$. [b] On the basis of all data.

angles of C(95)−Pt(1)−C(96) and C(99)−Pt(2)−C(100) at 178.79(18)° and 177.3(2)°, respectively.[59]

On the basis of the single-crystal structure of **Pt−1**, a rodlike geometry was found, with the B(2)−B(3) distance of 39.4989 Å. The two Pt(II) coordination centers are close to planar square geometry. For example, the P(1)−Pt(1)−P(2) bond angle is 173.44(5)°, and the C(109)−Pt(1)−C(110) bond angle is 176.80(18)°. The bond lengths of the acetylide C≡C bonds are in the range of 1.201−1.205 Å, which is close to the literature values.[59] Another distinct feature is the non-coplanar geometry of the styryl moiety with the Bodipy chromophore. For example, the dihedral angle of C(18)−C(19)−C(20)−C(21) is 18.998°, and the dihedral angle of C(26)−C(27)−-C(28)−C(33) is 0.127°. Furthermore, we found that the coordinated moieties on the long axial of the Pt(II) coordinated rod are not in a straight line. For example, C(110)−C(111)−C(112) is 176.0(5)°, C(111)−C(110)−Pt(1) is 173.2(4)°, C(123)−C(122)−Pt(2) is 173.3(5)°, and C(122)−C(123)−C(124) is 173.3(6)°. Similar deviation was also found for other *trans*-bis(trialkylphosphine) Pt(II) bisacetylides complexes.[53] In less congested Pt(II) complexes, a nearly straight coordination axial was found.[61] Similar geometries were observed for **Pt−0** (Tables S1 and S2, see Supporting Information).

UV−vis Absorption Spectra and Fluorescence Spectra. The UV−vis absorptions of the complexes were studied (Figure 2). The references **Pt−0** and **Pt−2**, which contain only the styrylBodipy or the Bodipy chromophore, give only *one* major absorption band at 734 or 504 nm, respectively. Notably, the absorption of the ligand **L−1** is red-shifted by 86 nm upon coordination with Pt(II). For **Pt−2**, however, the absorption wavelength is similar to the free ligand **L−2**. The different absorption of the two complexes is due to the derivatization

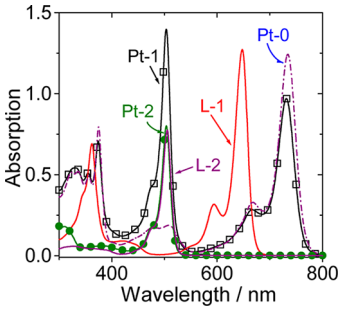

Figure 2. UV−vis absorption spectra of the compounds. $c = 1.0 \times 10^{-5}$ M in toluene, 20 °C.

position of the ethynyl on Bodipy moiety and thus the different perturbation on the π-conjugation framework of the chromophore.

For **Pt−1**, which contains *two* different types of Bodipy ligands as visible-light-harvesting antenna, two major absorption bands were observed at 503 and 731 nm (Figure 2). The absorption maxima of **Pt−1** is the sum of **Pt−0** and **Pt−2**; thus, there is no significant electronic interaction between the two kinds of Bodipy ligands in **Pt−1** at the ground state. Moreover, there is no π-conjugation across the Pt(II) atoms, otherwise the absorption wavelength of **Pt−1** will be drastically different from that of **Pt−0** and **Pt−2**. This finding is different from a previous result that delocalized Franck−Condon singlet-excited state was proposed.[25] To the best of our knowledge, *trans*-bisphosphine Pt(II) bisacetylide complexes showing near-IR absorption, like **Pt−1**, were not reported.[55,62,63] Recently we prepared N^N Pt(II) bisacetylide complex with heteroleptic acetylide ligands.[56] But the complex does not show any absorption in near-IR range.

Notably the complexes **Pt−0**, **Pt−1**, and **Pt−2** show very strong absorption in visible region, which was rarely reported for *trans*-bisphosphine Pt(II) bisacetylide complexes.[53,55,62−64] For example, the molar absorption coefficients (ε) of **Pt−1** at 503 and 731 nm are 1.4×10^5 M^{-1} cm^{-1} and 9.7×10^4 M^{-1} cm^{-1}, respectively.

The UV−vis absorption spectra and the luminescence spectra of the compounds were studied (Figure 3). For ligand **L−1**, emission band at 663 nm was observed (Figure 3a), which is a mirror to the absorption band on lower-energy side. The lifetime of the emission was determined as 5.55 ns. Note the small Stokes shift of the emission is typical for Bodipy fluorophores.[50,65−67] For **Pt−0**, the emission band is at 758 nm (Figure 3b). The small Stokes shift and the short luminescence lifetime of **Pt−0** (1.84 ns) indicated that the emission of **Pt−0** is fluorescence of the coordinated styrylBodipy ligand, not phosphorescence.[46] This result reveals the interesting photophysics of Pt(II) complexes; that is, no phosphorescence was observed even with *two* Pt(II) atoms coordinated to the π-conjugation framework of the same styrylBodipy ligand, which is in stark contrast to a previous observation that strong room-temperature (RT) phosphorescence of Bodipy ligand was observed with a N^C^N auxiliary coordination ligand (Φ_P = 3.5%).[29]

For **Pt−1**, two emission bands were observed (Figure 3c). The small Stokes shifts and the short luminescence lifetimes of the two emission bands (2.22 and 1.95 ns) suggest that the emission bands are fluorescence. Previously we prepared a Pt(II) complex that contains two different coordinated Bodipy

DOI: 10.1021/acs.inorgchem.5b01107
Inorg. Chem. 2015, 54, 7492−7505

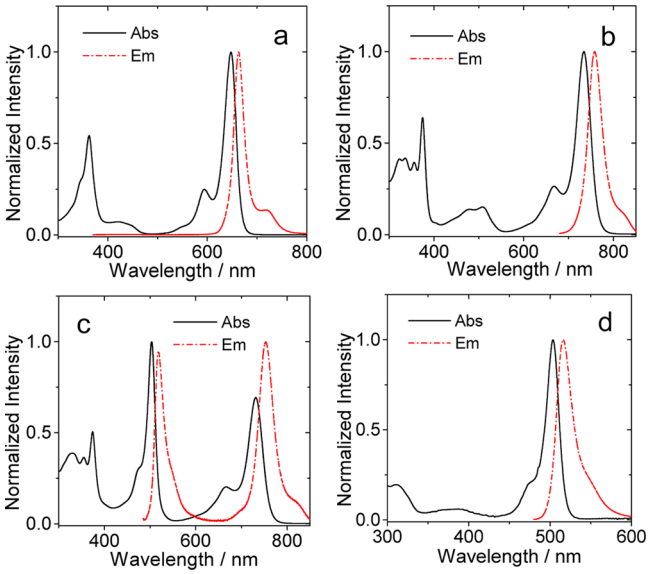

Figure 3. Comparison of the normalized UV−vis absorption spectra and emission spectra of (a) **L−1** (λ_{ex} = 362 nm), (b) **Pt−0** (λ_{ex} = 670 nm), (c) **Pt−1** (λ_{ex} = 480 nm), (d) **Pt−2** (λ_{ex} = 470 nm). c = 1.0 × 10^{-5} M in toluene, 20 °C.

ligands; only the fluorescence of the energy acceptor was observed.[43]

We propose a through-bond singlet-energy-transfer for **Pt−1**,[48] instead of the resonance energy transfer, since the emission of the peripheral Bodipy ligand overlap *poorly* with the absorption band of the central coordinated styrylBodipy ligand. The poor spectral overlap between the singlet-energy donor and the energy acceptor may result in inefficient FRET. Similar emission band with small Stokes shift was observed for **Pt−2** (Figure 3d). The emission band can be attributed to the fluorescence emission of the Bodipy ligand.

The solvent polarity-dependency of the UV−vis absorptions of the compounds were studied (Figure S21, see Supporting Information). No substantial changes were observed for the UV−vis absorption of the compounds with variation of the solvent polarity. Thus, we conclude that there is no substantial interaction or charge transfer for the compounds at ground states. The Franck−Condon states of the compounds were not affected by the solvent polarity. The solvent dependency of the luminescence of the compounds was studied (Figure S22, see Supporting Information). For ligand **L−1**, the emission intensity and wavelength do not change significantly with variation of the solvent polarity. For the coordinated **L−1**, that is, complex **Pt−0**, however, the emission intensity is dependent on the solvent polarity; the emission intensity was reduced in polar solvents as compared with that in nonpolar solvents such as toluene.

It should be pointed out that the quenched luminescence intensity of **Pt−1** in polar solvents is unlikely due to intramolecular charge transfer (ICT); otherwise, the emission wavelength of the emission bands will change substantially with variation of the solvent polarity.[68] The photophysical properties of the compounds were summarized in Table 2.

Electrochemical Studies: Cyclic Voltammetry. The electrochemical properties of the complexes were studied by cyclic voltammetry versus Fc(+/0) (Figure 4). For the

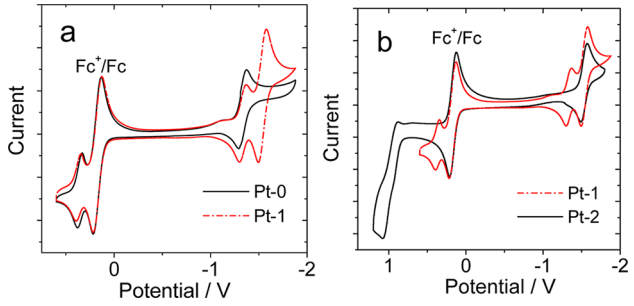

Figure 4. Cyclic voltammogram of **Pt−1**, **Pt−0**, and **Pt−2**. Ferrocene (Fc) was used as internal reference ($E_{1/2}$ = +0.17 V, Fc^+/Fc). In deaerated DCM solution containing 0.5 mM photosensitizers with the ferrocene, 0.10 M $Bu_4N[PF_6]$ as supporting electrolyte, Ag/$AgNO_3$ reference electrode, scan rates: 100 mV/s. 20 °C.

reference complex **Pt−0**, a reversible oxidation wave was observed for which the half-wave potential $E_{1/2}$ is +0.18 V, whereas in the cathodic scan, a reversible reduction was observed in which the half-wave potential $E_{1/2}$ is −1.51 V (Figure 4a). For **Pt−2**, a reversible reduction wave was observed for which the half-wave potential $E_{1/2}$ is −1.70 V, whereas in the oxidation region, an irreversible oxidation wave was observed in which the potential is +0.91 V (Figure 4b).

For **Pt−1** in the cathodic scanning, two reversible waves at −1.50 and −1.70 V were observed, which is the sum of the reduction waves of the reference complexes **Pt−0** and **Pt−2**. In the anode region, a reversible oxidation wave at +0.20 V was observed for **Pt−1**. This result indicates that there is no electronic interaction between the chromophores in **Pt−1**; otherwise, the reduction potentials of **Pt−1** should be

Table 2. Photophysical Properties of the Ligands and the Pt(II) Complexes[a]

	λ_{abs},[a] nm	ε[b]	λ_{em},[a] nm	Φ_F, %	Φ_Δ, %	τ_F,[c] ns	τ_T,[d] μs
L−1	362/648	6.9/12.7	663	23.6[e]	*f*	5.55	*f*
Pt−0	734	12.4	758	2.26[g]	37.0 ± 0.6[h]	1.84	5.82
Pt−1	503/731	14.0/9.7	518/754	1.46[i]/1.77[i]/2.65[g]	89.0 ± 1.3[j]/27.8 ± 0.4[h]	2.22/1.95	6.09
Pt−2	504	7.7	516	36.7[i]	12.1 ± 0.2[j]	2.67	708.55

[a]In toluene (c = 1.0 × 10^{-5} M). [b]Molar absorption coefficient. ε: 1 × 10^4 M^{-1} cm^{-1}. [c]Luminescence lifetimes. c = 1.0 × 10^{-5} M. [d]Triplet state lifetimes. c = 1.0 × 10^{-5} M, in deaerated toluene. [e]Fluorescence quantum yields. **B−7** (Φ_F = 9.3%) was used as standard for **L−1** (λ_{ex} = 584 nm). [f]Not applicable. [g]Fluorescence quantum yields. **B−3** (Φ_F = 9.5%) was used as standard for **Pt−0** and **Pt−1** (λ_{ex} = 640 nm). For **Pt−1** the fluorescence quantum yield belongs to the emission band at 754 nm. [h]Singlet oxygen quantum yields. Methylene blue (**MB** Φ_Δ = 57% in DCM) was used as standard for **Pt−0** and **Pt−1** (λ_{ex} = 670 nm). [i]Fluorescence quantum yields. **B−0** (Φ_F = 72% in THF) was used as standard for **Pt−1** (λ_{ex} = 483 nm) and **Pt−2** (λ_{ex} = 470 nm). For **Pt−1**, the first quantum yield is for the emission at 518 nm, and the second quantum yield is for the emission at 754 nm. [j]Singlet oxygen quantum yields, in toluene. Rose Bengal (**RB** Φ_Δ = 80% in MeOH) was used as standard for **Pt−1** and **Pt−2** (λ_{ex} = 516 nm).

DOI: 10.1021/acs.inorgchem.5b01107
Inorg. Chem. 2015, 54, 7492−7505

substantially different from that of the reference compounds. The redox potentials of the complexes were summarized in Table 3.

Table 3. Electrochemical Potentials Versus Fc(+/0)[a]

compound	oxidation, V	reduction, V
Pt−0	+0.18	−1.51
Pt−1	+0.20	−1.50, −1.70
Pt−2	+0.91	−1.70

[a]Cyclic voltammetry in deaerated DCM containing a 0.10 M Bu_4NPF_6 supporting electrolyte; counter electrode is Pt electrode; working electrode is glassy carbon electrode; $Ag/AgNO_3$ couple as the reference electrode. $[Ag^+]$ = 0.1 M, 0.5 mM photosensitizers in deaerated DCM. 20 °C.

Intramolecular photoinduced electron transfer may exert significant effect on the photophysical properties of multichromophore transition metal complexes, such as the luminescence property or the triplet-state property.[69−72] The Gibbs free energy changes (ΔG_{CS}) of the photoinduced electron transfer were calculated with the Rehm−Weller equation.[72,73] The results show that the electron transfer in **Pt−1** is thermodynamically prohibited (Table 4). This conclusion is in agreement with the spectroscopy studies.

Table 4. Free Energy Changes of Charge Recombination (ΔG_{CR}), Charge Separation (ΔG_{CS}), and Charge Separated States Energy Level (E_{CST}) of Pt−1 with the Coordinated StyrylBodipy as the Electron Donor and the Peripheral Bodipy as the Electron Acceptor[a]

electron transfer	ΔG_{CR}, eV	ΔG_{CS}, eV	E_{CST}, eV
^{1}StyrylBodipy* → Bodipy[b]	−2.32[c]	+0.67[c]	+2.32[c]
	−1.81[d]	+0.16[d]	+1.81[d]
	−1.67[e]	+0.02[e]	+1.67[e]
^{3}StyrylBodipy* → Bodipy[b]	−2.32[c]	+1.37[c]	+2.32[c]
	−1.81[d]	+0.86[d]	+1.81[d]
	−1.67[e]	+0.72[e]	+1.67[e]

[a]The arrow means the direction of charge transfer. [b]Electron transfer process in **Pt−1**. [c]In toluene. [d]In dichloromethane. [e]In MeCN.

Intramolecular Energy and Electron Transfer. To study the photoinduced electron transfer in **Pt−1**, the emission intensity of **Pt−0** and **Pt−1** was compared (Figure 5). Given an electron transfer occurred after photoexcitation, the fluorescence emission intensity of **Pt−1** should be weaker than that of

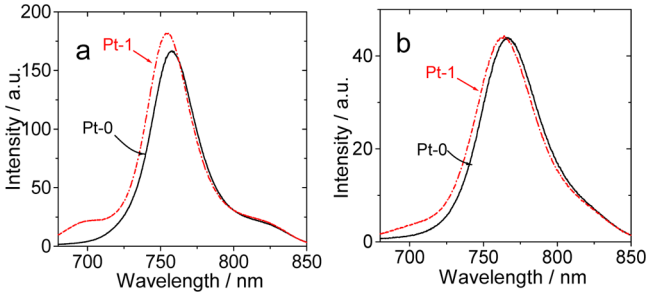

Figure 5. Fluorescence emission spectra of **Pt−0** and **Pt−1** (λ_{ex} = 670 nm, optically matched solutions were used) in different solvents of (a) toluene and (b) MeCN. 20 °C.

Pt−0; note that **Pt−0** is an analogue of the energy acceptor in **Pt−1**.

However, the experiments demonstrated that the fluorescence emission intensity of **Pt−1** is similar to that of **Pt−0** (Figure 5a; optically matched solutions were used). Similar results in solvents with different polarity were observed (Figure S23, see Supporting Information). Same result was observed even in polar solvent such as acetonitrile (Figure 5b). It is known that electron transfer is more favored in polar solvents. Therefore, we conclude that there is no significant photoinduced electron-transfer process in **Pt−1**,[70,74,75] which is in agreement with the electrochemical studies and the Gibbs free energy changes (ΔG_{CS}) of the electron transfer.

To study the energy-transfer process in **Pt−1**, the fluorescence intensities of **Pt−2** and **Pt−1** were compared (Figure 6). **Pt−2** is the analogue of the energy donor unit in

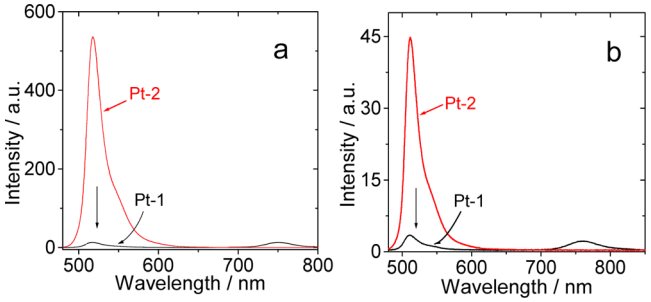

Figure 6. Fluorescence emission spectra of **Pt−1** and **Pt−2** (λ_{ex} = 473 nm; optically matched solutions were used) in (a) toluene and (b) MeCN. 20 °C.

Pt−1. It was found that the fluorescence emission intensity of **Pt−2** was significantly quenched in **Pt−1**. This quenching effect of the fluorescence of the peripheral Bodipy ligand is attributed to energy transfer, since we proved with the Gibbs free energy changes (ΔG_{CS}) that intramolecular electron transfer is prohibited in **Pt−1**.[74]

Same quenching effect was observed in toluene, as well as in dichloromethane (DCM), MeCN, and MeOH; thus, this quenching effect is unlikely due to polarity-enhanced ICT effect (Figure S24, see Supporting Information). The EnT rate constants were estimated at $k_{EnT} = 9.0 \times 10^9$ s^{-1} using eq 5.[74] This predicted value agrees with the femtosecond transient absorption spectroscopy ($k_{EnT} = 2.2 \times 10^{10}$ s^{-1}, see later section). This value is smaller as compared with the previously reported 7.8×10^{11} s^{-1} for a Bodipy−Pt(II) porphyrin complex.[76] For a Bodipy−AzaBodipy triad, for which the spectral overlap between the emission of the energy donor and the absorption of the energy acceptor is not significant, the rate constant of the EnT is 1.2×10^{11} s^{-1}.[70] These large FRET rate constants, despite the poor spectral overlap, may be attributed to through-bond-energy-transfer (TBET).[77−80]

Recently Akkaya et al. proposed to use the fluorescence excitation spectra to evaluate the singlet EnT efficiency.[75] Thus, the fluorescence excitation spectra of the compounds were studied. The excitation spectra of the compounds were recorded (Figure 7). For **Pt−1**, the excitation at 503 nm is half of the UV−vis absorption; therefore, we propose the FRET efficiency is ca. 50%. We noted the discrepancy for the EnT efficiency evaluated by the luminescence quenching and the excitation spectra.[81] However, the comparison of the excitation spectra with the UV−vis absorption spectrum in Figure 7

DOI: 10.1021/acs.inorgchem.5b01107
Inorg. Chem. 2015, 54, 7492−7505

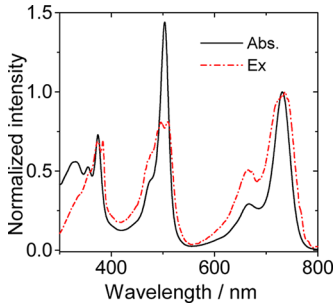

Figure 7. Comparison of the normalized UV−vis absorption and the luminescence excitation spectra of **Pt−1** (λ_{em} = 770 nm). c = 1.0 × 10^{-5} M in toluene at 20 °C.

unambiguously confirmed that there is singlet energy transfer from the peripheral Bodipy ligands to the central coordinated styrylBodipy ligand.[70,74,75]

Nanosecond Transient-Absorption Spectroscopy. To study the triplet-excited state of the complexes, the nanosecond transient-absorption spectroscopy of the complexes was studied (Figure 8).[58,82,83] For **Pt−0**, significant bleaching band at 741 nm was observed upon nanosecond pulsed laser excitation. Minor bleaching band at 369 nm was also observed; thus, the T_1 triplet state of **Pt−0** is localized on the Bodipy unit. The transient was significantly quenched in aerated solution (Figure S25a, see Supporting Information). Thus, the signal can be attributed to the triplet state of the complex.

The triplet-state lifetime was determined as 5.8 μs, which is much shorter than a similar *trans*-bis(trialkylphosphine) bisacetylide complex with Bodipy ligand (not styrylBodipy ligand. τ_T = 128 μs).[29] However, this lifetime is close to that observed with heavy atom effect (τ_T = 1.8 μs).[84] Previously we prepared a C_{60}−styrylBodipy dyad, for which a much longer triplet-state lifetime was observed (71−123 μs).[85] The different triplet-state lifetime may be due to the different steric hindrance of the styryl moiety; with bulky substitution on the 2,6-position, the coplanarity of the π-conjugation framework is compromised (which is confirmed by the molecular structures determined with the single-crystal X-ray diffraction). As a result, the lifetime of the triplet state of styrylBodipy was reduced.

For **Pt−2**, significant bleaching band at 504 nm was observed upon nanosecond pulsed laser excitation at 503 nm (Figure 8e). The lifetime was determined as 709 μs. Thus, we conclude that the triplet-excited state is localized on the Bodipy moiety.

For **Pt−1**, as previously confirmed, singlet-energy transfer from the peripheral Bodipy ligands to the central coordinated styrylBodipy ligand occurs. Thus, **Pt−1** was selectively excited into the peripheral coordinated Bodipy parts (λ_{ex} = 500 nm). Interestingly, no bleaching band at 504 nm was observed, which is different from **Pt−2**. Instead, intensive bleaching band at 741 nm was observed, which is similar to **Pt−0**. Thus, we conclude that triplet state is confined on the central coordinated Bodipy ligand upon selective excitation into the peripheral Bodipy part.[86] Since we confirmed the triplet-state formation in **Pt−2**, and the fact that no triplet state is localized on the peripheral Bodipy in **Pt−1**, we propose that intramolecular triplet−triplet-energy transfer (TTET) exists for **Pt−1**. Since no increasing stage was observed for the transient signal at 741 nm, we propose the triplet state EnT in **Pt−1** is fast ($k \gg 1 \times 10^8$ s^{-1}. The time-resolution of the nanosecond transient absorption spectrometer is 10 ns). Previously it was reported that the intramolecular triplet-state energy-transfer rate constant is 1.0 × 10^{10} s^{-1} for a Bodipy−Pt(porphyrin) complex.[76]

The above result confirms that the excitation energy harvested by the energy donor, that is, the peripheral coordinated Bodipy part, can be funneled efficiently into the energy acceptor, either through intramolecular singlet energy transfer or TTET. **Pt−1** was also excited with pulsed laser at

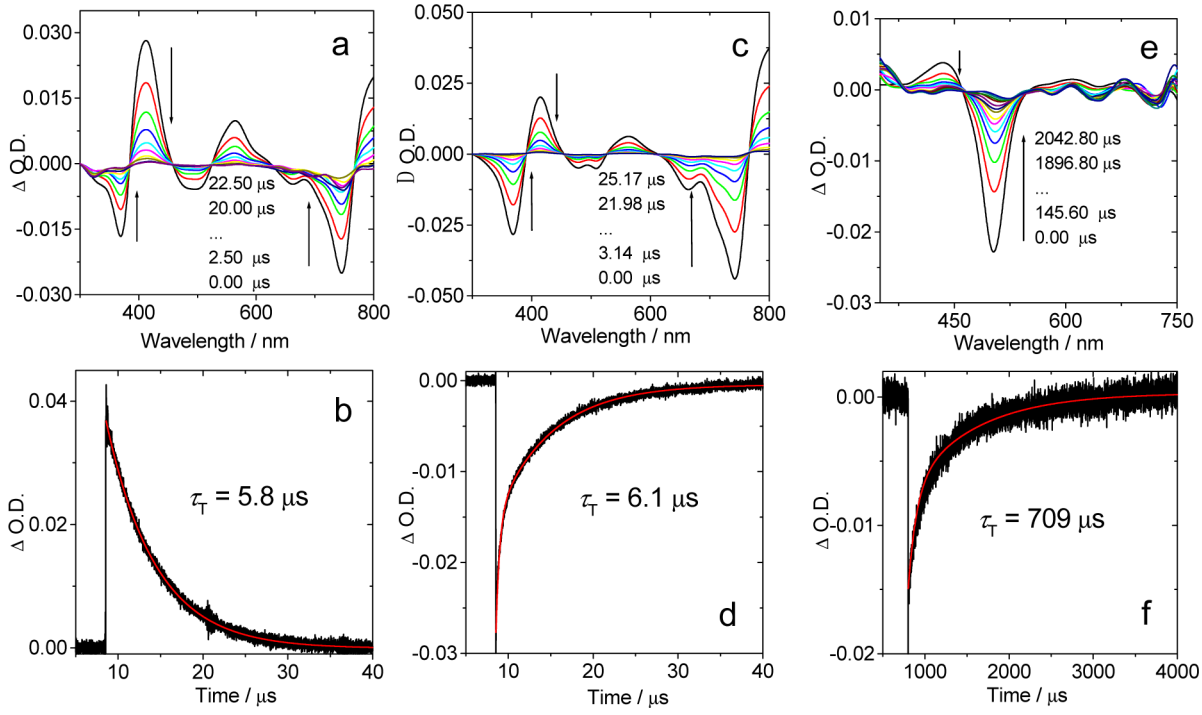

Figure 8. Nanosecond transient absorption spectra. (a) **Pt−0** and (b) decay curve at 420 nm (λ_{ex} = 510 nm); (c) **Pt−1** and (d) decay curve at 490 nm (λ_{ex} = 500 nm); (e) **Pt−2** and (f) decay curve at 490 nm (λ_{ex} = 503 nm). c = 1.0 × 10^{-5} M in deaerated toluene at 20 °C.

DOI: 10.1021/acs.inorgchem.5b01107
Inorg. Chem. 2015, 54, 7492−7505

725 nm, that is, selectively into the energy-acceptor part. Exactly the same transient spectra was observed, and the triplet-state lifetime was determined as 6.5 μs (Figure S26, see Supporting Information).

The triplet-state property of **Pt−1** in polar solvent such as acetonitrile was studied (Figure 9). Triplet-excited state was

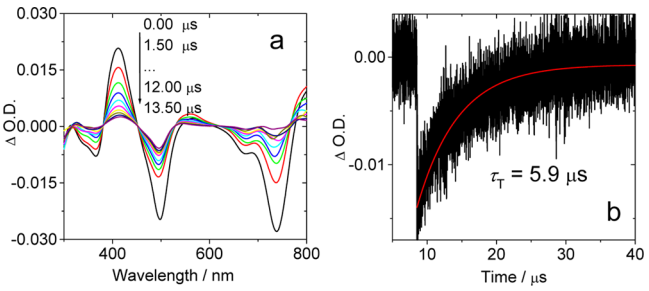

Figure 9. (a) Nanosecond transient absorption spectra of **Pt−1**; (b) decay curve of **Pt−1** at 490 nm (λ_{ex} = 500 nm). c = 1.0 × 10^{-5} M in deaerated MeCN at 20 °C.

observed with lifetime of 5.9 μs, which is close to the triplet-state lifetime in nonpolar solvent such as toluene (6.1 μs, Figure 8d). Thus, the photoinduced electron-transfer effect in **Pt−1** is not significant, which is in agreement with the study of the Gibbs free energy changes (Table 4) and the fluorescence spectra (Figure 5). A recently reported broadband visible-light-absorbing N^N Pt(II) bisacetylide complex with heteroleptic acetylide ligands shows longer triplet-state lifetime of 68.21 μs.[56]

The triplet state of the ligand **L−1** was produced with the sensitization method; that is, 2,6-diiodoBodipy (**B−2**, Scheme 1) was used as the triplet-state energy donor (photosensitizer) and **L−1** as the triplet-state energy acceptor (Figure 10).[87]

The triplet-state lifetime of **B−2** was reduced to 22.8 μs in the presence of **L−1**. Note the intrinsic triplet-state lifetime of **B−2** is 179.8 μs (Figure S27, see Supporting Information). The bleaching band at 647 nm was determined with a lifetime of 152 μs, which is much longer than that of **Pt−1**. This value is close to a previously reported triplet-state lifetime of styrylBodipy compounds observed with C_{60}−StyrylBodipy dyads, that is, intramolecular sensitization method (71.5−123.2 μs).[91]

Long-range energy transfer is important in photosynthesis.[87,88] Normally long-range intermolecular energy transfer is inefficient. For example, FRET will not occur for the mixture of the energy donor and energy acceptor in solution.[89] Intermolecular triplet-state energy transfer is rarely studied.[87] Intermolecular triplet-state energy transfer is normally inefficient due to the short lifetime of the excited state of the energy donor. For **Pt−2**, however, the triplet-state lifetime is very long (709 μs); thus, long-range intermolecular triplet-energy transfer with **Pt−2** is possible. To study the triplet-energy transfer in **Pt−1**, complex **Pt−2** was also used as triplet-state energy donor, and the ligand **L−1** was used as triplet-state energy acceptor. This mixture can be used as a model for studying of the triplet-state energy transfer in **Pt−1**.

With increasing concentration of **L−1**, the lifetime of the bleaching band at 504 nm was reduced, and a new bleaching band at 642 nm was observed (Figure 11, and Supporting

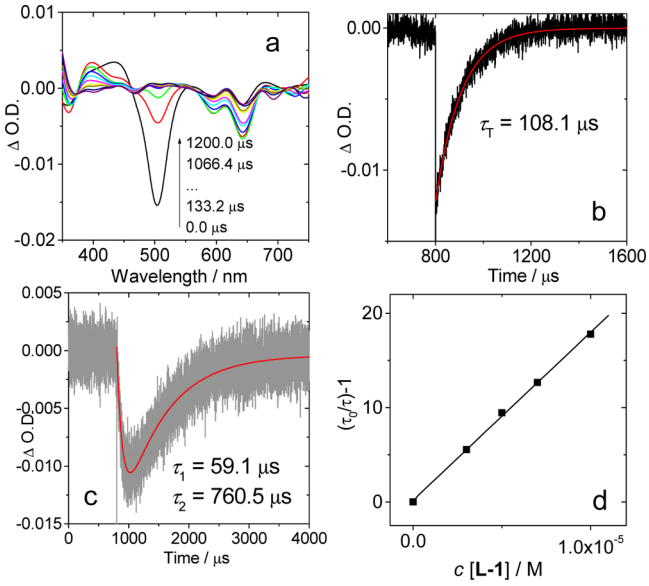

Figure 11. Nanosecond transient absorption spectra and the decay curves of the mixture of complex **Pt−2** and ligand **L−1**. (a) Molar ratio is 1:0.3 (**Pt−2**/**L−1**); decay curves at (b) 490 nm and (c) 640 nm (λ_{ex} = 503 nm), molar ratio is 1:0.3 (**Pt−2**/**L−1**); (d) Stern−Volmer plots for lifetime quenching of **Pt−2** with increasing the concentration of **L−1**. λ_{ex} = 503 nm. [**Pt−2**] = 1.0 × 10^{-5} M. In deaerated toluene at 20 °C.

Information Figure S28). The change of the transient absorption spectra upon increasing the triplet-energy acceptor **L−1** was attributed to the intermolecular triplet-energy transfer and the produce of the triplet state of **L−1**.

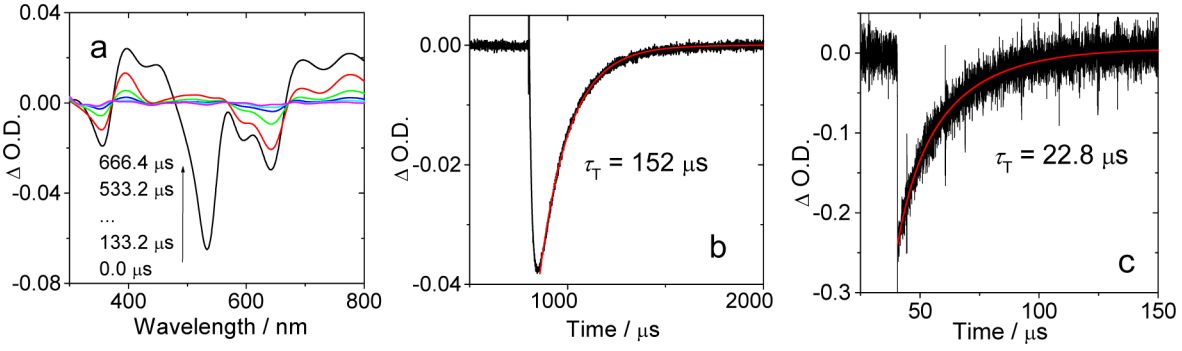

Figure 10. (a) Nanosecond time-resolved transient absorption spectra of the mixture of **B−2** (sensitizer) and **L−1** (triplet-energy acceptor). (b) Decay curve at 647 nm (λ_{ex} = 528 nm) and (c) decay curve at 532 nm (λ_{ex} = 528 nm). c = 1.0 × 10^{-5} M in deaerated toluene at 20 °C.

DOI: 10.1021/acs.inorgchem.5b01107
Inorg. Chem. 2015, 54, 7492−7505

To study the kinetics of the intermolecular energy transfer, the decay trace at 640 nm was monitored. Interestingly, the decay is featured with biphase character; that is, there is first a sharp increase of the bleaching at 640 nm, and then a slow decay process was observed (Figure 11c). Similar results were observed in Figure 10b. The fast increase of the transient is attributed to the production of the triplet state of **L−1** via the intermolecular triplet-energy transfer, and thereafter the relatively slow decay of the transient is attributed to the decay of the triplet state of **L−1**. The exceptionally long lifetime of the triplet state is probably due to the low concentration of **L−1** molecule at triplet state. The triplet-state intermolecular energy-transfer rate constant was calculated as on 1 × 10^4 s^{-1} scale (which is concentration-dependent) according to eq 6 (Table 5). The triplet-state energy-transfer efficiency was calculated as ca. 92% according to eq 7. These values are similar to that observed with intra-assembly (hydrogen-bonded molecular assembly) triplet-state energy transfer in a C_{60}−ferrocene hydrogen-bonding molecular assembly (9.2 × 10^5 s^{-1}), which indicates that the intermolecular triplet-energy transfer is efficient.[88] Previously a sub-phthalocyanine/zinc tetra-*tert*-butylphthalocyanine triplet-state energy transfer was observed to show similar triplet-state energy transfer k = 4.2 × 10^5 s^{-1}.[87]

Table 5. Rate Constant (k_{ET}) and Efficiency (Φ_{ET}) for the Triplet−Triplet Energy Transfer in the Mixture of Pt−1 and Pt−2[a]

Pt−2/L−1	k_{ET} (s^{-1})	Φ_{ET} (%)
1.0:0.3	1.6 × 10^4	92.2
1.0:0.5	2.0 × 10^4	92.3
1.0:0.7	2.4 × 10^4	91.4
1.0:1.0	3.6 × 10^4	94.5

[a]In deaerated toluene. 20 °C.

The Stern−Volmer quenching constant of **Pt−2/L−1** was calculated as K_{SV} = 1.78 × 10^6 M^{-1} (Figure 11d). The bimolecular quenching constant was calculated as 2.5 × 10^9 M^{-1} s^{-1} according to eq 8. Quenching efficiency was given by eq 9, where k_0 is the diffusion-controlled bimolecular quenching rating constants, which can be calculated with the Smoluchowski eq 10.[89]

The molecular radius of the energy donor (**Pt−2**) is 8.7 Å, and that of quencher (**L−1**) is 8.6 Å. According to eq 11 the diffusion coefficient of the energy donor (**Pt−2**) is 4.21 × 10^{-6} cm^2 s^{-1}, and that of the quencher (**L−1**) is 4.26 × 10^{-6} cm^2 s^{-1} (in deaerated toluene at 20 °C). Thus, k_0 was calculated as 1.11 × 10^{10} M^{-1} s^{-1}. The quenching efficiency was calculated as 22.7% according to eq 9, which indicates that there is an efficient triplet-state energy transfer between **Pt−2** and **L−1** in the mixture.

Femtosecond Transient Absorption Spectroscopy. Ultrafast pump−probe experiments were performed for study of the singlet EnT (Figure 12). Ultrafast pump−probe experiments were performed for **Pt−0**, **Pt−1**, and **Pt−2** at appropriate pump wavelengths (Figures 12 and 13 and Supporting Information, Figures S29−S33). It is expected that singlet EnT may occur only for **Pt−1**, which contains two different kinds of Bodipy unit. Upon excitation of **Pt−1** at 505 nm, bleaching bands were observed around 505 and 730 nm, where the Bodipy and styrylBodipy give steady-state absorption, respectively (Figure 12). Transient absorption

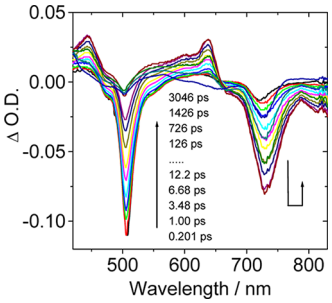

Figure 12. Femtosecond transient absorption spectra of **Pt−1** (λ_{ex} = 505 nm). c = 1.0 × 10^{-5} M in deaerated toluene at 20 °C.

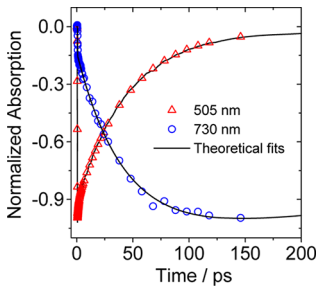

Figure 13. Decay curves of **Pt−1** at 505 and 730 nm (λ_{ex} = 505 nm). c = 1.0 × 10^{-5} M in deaerated toluene at 20 °C.

spectra of **Pt−1** show that the bleaching signal around 505 nm decreases, while the bleaching signal around 730 nm increases, simultaneously.

The decay time of the bleaching signal for Bodipy (505 nm) is ∼45 ps (k_{EnT} = 2.2 × 10^{10} s^{-1}), which is approximately equal to the rise time of the bleaching signal for styrylBodipy (730 nm) in **Pt−1** (Figure 13). These results give strong evidence of singlet EnT from Bodipy to styrylBodipy. Previously a Bodipy−AzaBodipy triad was studied, for which the spectral overlap between the emission of the energy donor and the absorption of the energy acceptor is not significant; the rate constant of the EnT is 1.2 × 10^{11} s^{-1}.[70] Recently we prepared N^N Pt(II) bisacetylide complex with heteroleptic acetylide ligands.[56] The singlet-energy transfer rate constant is 10-fold faster, 2.6 × 10^{11} s^{-1}.

The positive signal (excited-state absorption, ESA) represents $S_1 \rightarrow S_n$ transition of Bodipy and styrylBodipy and $T_1 \rightarrow T_n$ transition of styrylBodipy. The ESA signals around 430 and 620 nm can be attributed to $S_1 \rightarrow S_n$ transition of Bodipy due to appearance of these signals at zero time delay upon excitation of Bodipy. The other ESA signals around 445 and 635 nm increased after singlet EnT process; therefore, these signals can be attributed to $S_1 \rightarrow S_n$ transition of styrylBodipy. In addition to that, evidence of $T_1 \rightarrow T_n$ transition is obtained from positive signals that were placed around 420 and 560 nm probe wavelengths. These signals appear after ∼1 ns.

We also checked whether any energy transfer from styrylBodipy to Bodipy with an extra pump−probe experiment upon excitation styrylBodipy (730 nm) for **Pt−1**. There are bleach signals of ground state (730 nm) and photoinduced charge-transfer state (810 nm) of styrylBodipy, and no energy transfer is seen as expected (Figures S29a and S31, see Supporting Information).

Density Functional Theory Computations. The ground-state geometry and the excited states of the near-IR absorbing complex **Pt−0** were studied with density functional theory

DOI: 10.1021/acs.inorgchem.5b01107
Inorg. Chem. 2015, 54, 7492−7505

(DFT) and time-dependent density functional theory (TDDFT) computations (Figure 14). The optimized P−Pt−P bond angles are 179.779° and 179.782°, which is similar to the structure determined with the single-crystal molecular structure. The C≡C bond lengths are in the range of 1.2277−1.2290 Å, also in agreement with the experimental values.

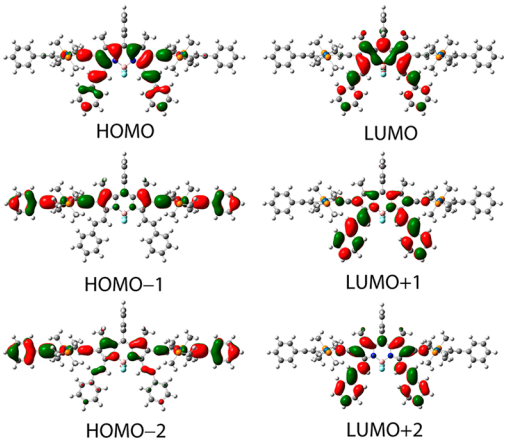

Figure 14. Electron density maps of the frontier molecular orbitals of **Pt−0** based on the optimized ground-state geometry. Calculated at the B3LYP/GENECP/LANL2DZ level with Gaussian 09W.

The singlet and triplet excited states of **Pt−0** were studied with TDDFT computations. The highest occupied molecular orbital (HOMO) and lowest unoccupied molecular orbital (LUMO) are involved in the low-lying excited states (S_1 state and T_1 state. Table 6). Thus, S_1 state, as well as the T_1 state, is localized on the coordinated styrylBodipy moiety, which is in agreement with the steady-state and the time-resolved transient absorption spectra of the complex. The spin density surface of **Pt−0** was also studied; the results show the spin density is localized on the coordinated Bodipy (Figure 15).

Singlet Oxygen Photosensitizing. The singlet oxygen ($^1O_2$) photosensitizing ability of the complexes was compared (Figure 16). 1,3-Diphenylisobenzofuran (DPBF) was used as $^1O_2$ scavenger for monitoring the $^1O_2$ production. First the $^1O_2$ photosensitizing ability of **Pt−0** and **Pt−1** was compared upon selective photoexcitation into the energy donor in **Pt−1**. At 503 nm, **Pt−1** shows stronger absorption than **Pt−0**. However, no enhanced $^1O_2$ photosensitizing should be observed given no energy transfer exists in **Pt−1**. The results show that **Pt−1** is more efficient than **Pt−0** to produce $^1O_2$ (Figure 16a). Thus, singlet EnT in **Pt−1** is confirmed.

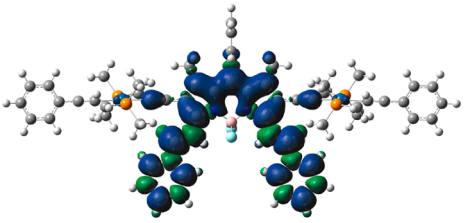

Figure 15. Isosurfaces of spin density of **Pt−0**. Calculated at the optimized triplet-state geometries at B3LYP/GENECP/LANL2DZ level with Gaussian 09W.

Similar results were obtained with white light excitation (Figure 16b). **Pt−1** is more efficient than **Pt−0** and **Pt−2** for production of $^1O_2$. These results confirm the singlet EnT in **Pt−1** and that the broadband absorption of **Pt−1** is advantageous for **Pt−1** to be used for photocatalysis.

The $^1O_2$ photosensitizing ability of **Pt−1** and **Pt−2** was also compared, upon excitation at the same wavelength (Figure 16c). The result shows that **Pt−1** is more efficient than **Pt−2** as $^1O_2$ photosensitizer upon excitation at 503 nm. Thus, intramolecular singlet EnT was confirmed for **Pt−1**, and the intersystem crossing is weak in **Pt−2**.

CONCLUSIONS

trans-Bis(tributylphosphine) Pt(II) bisacetylide complex (**Pt−1**) was prepared, which shows strong broadband visible-light/near-IR absorption at both 503 nm ($\varepsilon = 1.4 \times 10^5$ M^{-1} cm^{-1}) and 731 nm ($\varepsilon = 9.7 \times 10^4$ M^{-1} cm^{-1}). The complex contains two peripheral coordinated Bodipy ligands and a centrally coordinated styrylBodipy ligand, which show absorption at 503 and 731 nm, respectively. Reference complexes (**Pt−0** and **Pt−2**), which contain a *single* visible-light-harvesting Bodipy ligand, were prepared for comparison. The photophysical properties of the complexes were studied with steady-state and femtosecond/nanosecond time-resolved transient-absorption spectroscopies. Dual fluorescence at 518 and 754 nm was observed for **Pt−1**, which is rare for Bodipy-containing Pt(II) complexes. No phosphorescence was observed for **Pt−1**. With fluorescence emission spectra and excitation spectra, singlet EnT in **Pt−1** was confirmed (Φ_{EnT} = 50%). TBET mechanism was proposed to be responsible for the ultrafast singlet EnT in **Pt−1**, due to the poor spectral overlap, yet fast energy transfer. Femtosecond transient absorption indicated the intramolecular singlet EnT is

Table 6. Excitation Energies (eV) and Corresponding Oscillator Strengths (f), Main Configurations, and CI Coefficients of the Low-Lying Electronically Excited States of Pt−0, Calculated by TDDFT//B3LYP/LANL2DZ, Based on the DFT//B3LYP/LANL2DZ Optimized Ground-State Geometries

	TDDFT/B3LYP/LANL2DZ					
	electronic transition	energy [eV/nm][a]	f[b]	composition[c]	CI[d]	character
singlet	$S_0 \rightarrow S_1$	1.91/648	0.8572	H→L	0.6852	MLCT
	$S_0 \rightarrow S_3$	2.46/503	0.4345	H−2→L	0.6297	MLCT/ILCT
	$S_0 \rightarrow S_9$	3.28/378	0.8707	H→L+1	0.4953	MLCT
	$S_0 \rightarrow S_{19}$	3.73/333	0.6393	H−1→L+1	0.5331	MLCT/ILCT
triplet[e]	$S_0 \rightarrow T_1$	0.95/1311	0.0000	H→L	0.6989	MLCT
	$S_0 \rightarrow T_2$	1.92/645	0.0000	H−1→L	0.5501	MLCT/ILCT
	$S_0 \rightarrow T_3$	1.945/637	0.0000	H−2→L	0.4799	MLCT/ILCT

[a]Only the selected low-lying excited states are presented. [b]Oscillator strengths. [c]Only the main configurations are presented. [d]The CI coefficients are in absolute values. [e]No spin−orbital coupling effect was considered; thus, the f values are zero.

DOI: 10.1021/acs.inorgchem.5b01107
Inorg. Chem. 2015, 54, 7492−7505

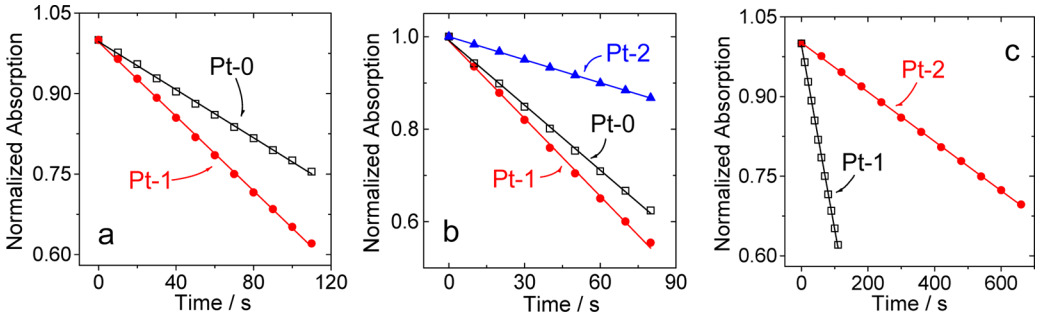

Figure 16. Comparison of the singlet oxygen ($^1O_2$) photosensitizing of (a) **Pt−0** and **Pt−1** (λ_{ex} = 503 nm). $c = 1.0 \times 10^{-5}$ M, respectively. (b) **Pt−0**, **Pt−1**, and **Pt−2** (xenon lamp was used as light source). [**Pt−0**] and [**Pt−1**] = 1.0×10^{-5} M; [**Pt−2**] = 2.0×10^{-5} M. (c) **Pt−1** and **Pt−2** (λ_{ex} = 503 nm, optically matched solutions were used), [**Pt−1**] = 1.0×10^{-5} M. In toluene. 20 °C.

fast: $k_{EnT} = 2.2 \times 10^{10}$ s^{-1}. Gibbs free energy changes (ΔG_{CS}) and steady-state luminescence studies show that the photoinduced intramolecular electron transfer in **Pt−1** is prohibited. With nanosecond time-resolved transient-absorption spectra, intramolecular triplet-state energy transfer was proved, and the T_1 state of **Pt−1** is only confined on the central coordinated Bodipy ligand. Intermolecular triplet-state energy transfer was studied with nanosecond time-resolved transient absorption spectra ($k_{EnT} = 3.6 \times 10^4$ s^{-1} and Φ_{EnT} = 94.5%). With singlet oxygen ($^1O_2$) photosensitizing experiments, we proved that the broadband visible-light-absorbing of **Pt−1** is beneficial for the complex to be used as triplet photosensitizers. These studies will be useful for designing near-IR absorbing Pt(II) complexes and for the application of these complexes in luminescent bioimaging and photodynamic therapy studies.

EXPERIMENTAL SECTION

Materials. Solvents were dried or distilled for synthesis. K_2PtCl_4 was purchased from Aladdin Chemical Co., Ltd. (P. R. China). **B−2** was synthesized according to literature methods.[58]

Analytical Measurements. All chemicals are analytically pure and used as received. NMR spectra were recorded by Bruker 500 MHz spectrometer and OXFPRD NMR 400 MHz spectrometer with $CDCl_3$ as solvent and tetramethylsilane (TMS) as standard at 0.00 ppm. HRMS was accomplished with GCT time-of-flight (TOF) mass spectrometer (Waters, U.K.) and matrix-assisted laser desorption/ionization (MALDI) micro MALDI TOF mass spectrometer (Waters, U.K.). Fluorescence spectra were measured on an RF5301 PC spectrofluorometer (Shimadzu, Japan). Absorption spectra were recorded on UV2550 UV−vis spectrophotometer (Shimadzu, Japan).

Synthesis of ***1****.*[90] K_2PtCl_4 (1.04 g, 2.5 mmol) was dissolved in 20 mL of deionized water under argon atmosphere (Ar). $P(^nBu)_3$ (1.07 g, 5.3 mmol) was injected. Then the mixture was stirred under Ar at room temperature (RT) for 3 h. After the reaction was finished, the solid was filtrated out and purified by column chromatography (silica gel, CH_2Cl_2). **1** was collected as a white solid (0.97 g, yield: 57.7%). ^1H NMR (400 MHz, $CDCl_3$): 2.02−1.96 (m, 12H), 1.55−1.50 (m, 12H), 1.49−1.40 (m, 12H), 0.95 (t, 18H, J = 7.2 Hz). TOF-HRMS ($[C_{24}H_{54}Cl_2P_2Pt]^+$): calcd m/z = 669.2726, found m/z = 669.2731.

Synthesis of ***2****.*[30] **1** (435 mg, 0.65 mmol) was dissolved in 30 mL of dried $NHEt_2$ under Ar. Phenylacetylene (61 mg, 0.60 mmol) was injected. Then the mixture was stirred under Ar at 45 °C for 8 h. After the reaction was finished, the solvent was removed under reduced pressure. The residue was purified by column chromatography (silica gel, CH_2Cl_2/petroleum ether (PE) = 1:5, v/v). **2** was collected as a light yellow solid (382 mg, yield: 79.8%). ^1H NMR (400 MHz, $CDCl_3$): 7.25−7.18 (m, 4H), 7.16−7.11 (m, 1H), 2.04−1.98 (m, 12H), 1.62−1.52 (m, 12H), 1.49−1.40 (m, 12H), 0.92 (t, 18H, J = 7.3 Hz). MALDI-TOF-HRMS ($[C_{32}H_{59}ClP_2Pt - Cl]^+$): calcd m/z = 700.3740, found m/z = 700.3727.

Synthesis of ***3****.*[84] **B−2** (28 mg, 0.05 mmol) was dissolved in 3 mL of dried dimethylformamide. Benzaldehyde (21 mg, 0.2 mmol) was added, followed by three drops of acetic acid and three drops of piperidine before the mixture was saturated by Ar. Then the mixture was subjected to microwave irradiation for 6 min at 150 °C under Ar. After the reaction was finished, 25 mL of water was added. The solid was filtrated out and purified by column chromatography (silica gel, CH_2Cl_2/PE = 1:4, v/v). **3** was collected as a dark green solid (32 mg, yield: 85.1%). ^1H NMR (400 MHz, $CDCl_3$): 8.16 (d, 2H, J = 16.7 Hz), 7.74−7.66 (m, 6H), 7.56−7.54 (m, 3H), 7.45−7.41 (m, 4H), 7.38−7.34 (m, 2H), 7.31−7.29 (m, 2H), 1.46 (s, 6H). MALDI-TOF-HRMS ($[C_{33}H_{25}BF_2I_2N_2]^+$): calcd m/z = 752.0168, found m/z = 752.0184.

Synthesis of ***4****.*[29] **3** (70 mg, 0.09 mmol) was dissolved in 5 mL of distilled tetrahydrofuran (THF) before 2.5 mL of $(^iPr)_2NH$ was added under Ar. $Pd(PPh_3)_2Cl_2$ (17 mg, 0.02 mmol) and PPh_3 (13 mg, 0.05 mmol) were added, followed by CuI (9.4 mg, 0.05 mmol). Trimethylsilylacetylene (35 mg, 0.36 mmol) was injected before the mixture was stirred under Ar for 6 h at 68 °C. After the reaction was finished, the solvent was removed under reduced pressure. The residue was purified by column chromatography (silica gel, CH_2Cl_2/PE = 1:4, v/v). **4** was collected as a dark green solid (48 mg, yield: 77.0%). ^1H NMR (400 MHz, $CDCl_3$): 8.44 (d, 2H, J = 16.3 Hz), 7.79 (d, 2H, J = 16.5 Hz), 7.65 (d, 4H, J = 7.5 Hz), 7.53−7.52 (m, 3H), 7.45−7.41 (m, 4H), 7.37−7.34 (m, 2H), 7.30−7.28 (m, 2H), 1.51 (s, 6H), 0.27 (s, 18H). ^{13}C NMR (100 MHz, $CDCl_3$): δ 152.7, 146.9, 140.4, 139.4, 136.8, 134.6, 132.5, 129.5, 129.4, 129.3, 128.8, 128.1, 127.8, 118.6, 112.9, 86.4, 29.7, 1.0. MALDI-TOF-HRMS ($[C_{43}H_{43}BN_2F_2Si_2]^+$): calcd m/z = 692.3026, found m/z = 692.3005.

Synthesis of ***L−1****.*[29] **4** (34.6 mg, 0.05 mmol) was dissolved in 3 mL of distilled THF. $Bu_4NF{\cdot}3H_2O$ (0.2 M in THF, 1 mL) was added dropwise at −78 °C under Ar, and the solution was kept at −78 °C for ∼0.5 h (monitored by thin-layer chromatography until the starting material had been completely consumed). After the reaction was finished, 20 mL of water and 30 mL of CH_2Cl_2 were added. The aqueous layer was extracted with CH_2Cl_2 (3 × 10 mL). The combined organic layers were dried over anhydrous Na_2SO_4. The solvent was removed under reduced pressure. The residue was purified by column chromatography (silica gel, CH_2Cl_2/PE = 1:4, v/v). **L−1** was collected as a dark green solid (16 mg, yield: 58.4%). ^1H NMR (400 MHz, $CDCl_3$): 8.37 (d, 2H, J = 16.6 Hz), 7.78 (d, 2H, J = 16.2 Hz), 7.67 (d, 4H, J = 7.6 Hz), 7.55−7.54 (m, 3H), 7.45−7.41 (m, 4H), 7.37−7.36 (m, 2H), 7.31−7.30 (m, 2H), 3.57 (s, 2H), 1.52 (s, 6H). ^{13}C NMR (100 MHz, $CDCl_3$): δ 152.5, 146.2, 140.0, 139.2, 137.0, 134.7, 132.6, 129.4, 129.3, 129.2, 128.8, 127.7, 118.8, 114.0, 104.1, 98.9, 77.2, 29.7. MALDI-TOF-HRMS ($[C_{37}H_{27}BF_2N_2]^+$): calcd m/z = 548.2235, found m/z = 548.2269.

Synthesis of ***Pt−0****.*[28] **2** (30 mg, 0.04 mmol) and **L−1** (10 mg, 0.02 mmol) were dissolved in the mixture of distilled THF (2 mL) and dried $NHEt_2$ (2 mL) under Ar. CuI (2 mg, 0.01 mmol) was added before the mixture was stirred for 0.5 h at RT. After the reaction was finished, 20 mL of water and 30 mL of CH_2Cl_2 were added. The aqueous layer was extracted with CH_2Cl_2 (3 × 15 mL). The combined

DOI: 10.1021/acs.inorgchem.5b01107
Inorg. Chem. 2015, 54, 7492−7505

organic layers were dried over anhydrous Na_2SO_4. The solvent was removed under reduced pressure. The residue was purified by column chromatography (silica gel, CH_2Cl_2/PE = 1:3, v/v). **Pt−0** was collected as a dark green solid (22 mg, yield: 61.9%). Crystals were obtained by slow liquid diffusion of *n*-hexane into a concentrated CH_2Cl_2 solution. ^{1}H NMR (400 MHz, $CDCl_3$): 8.93 (d, 2H, J = 16.5 Hz), 7.82 (d, 2H, J = 16.5 Hz), 7.62 (d, 4H, J = 7.8 Hz), 7.48 (t, 3H, J = 5.5 Hz), 7.37−7.27 (m, 12H), 7.20 (t, 4H, J = 15.3 Hz), 7.11 (t, 2H, J = 15.0 Hz), 2.09−2.03 (m, 24H), 1.55−1.50 (m, 24H), 1.43 (s, 6H), 1.37−1.27 (m, 24H), 0.82 (t, 36H, J = 14.5 Hz). ^{13}C NMR (100 MHz, $CDCl_3$): δ 150.8, 140.8, 138.0, 137.6, 137.1, 136.3, 133.2, 131.0, 129.2, 129.0, 128.9, 128.7, 128.5, 128.0, 127.7, 125.0, 120.1, 120.0, 119.8, 119.6, 109.7, 108.2, 108.0, 107.9, 102.5, 29.9, 26.5, 24.6, 24.5, 24.4, 24.3, 24.1, 24.0, 13.9. MALDI-TOF-HRMS ($[C_{101}H_{143}BF_2N_2P_4Pt_2]^+$): calcd m/z = 1946.9559, found m/z = 1946.9431.

Synthesis of ***Pt−1****.*[28] **Pt−2** (30 mg, 0.03 mmol) and **L−1** (8 mg, 0.015 mmol) were dissolved in the mixture of distilled THF (3 mL) and dried $NHEt_2$ (3 mL) under Ar. CuI (3 mg, 0.015 mmol) was added before the mixture was stirred for 3 h at RT. After the reaction was finished, 20 mL of water and 30 mL of CH_2Cl_2 were added. The aqueous layer was extracted with CH_2Cl_2 (3 × 15 mL). The combined organic layers were dried over anhydrous Na_2SO_4. The solvent was removed under reduced pressure. The residue was purified by column chromatography (silica gel, CH_2Cl_2/PE = 1:1, v/v). **Pt−1** was collected as a dark green solid (16 mg, yield: 43.0%). Crystals were obtained by slow liquid diffusion of *n*-hexane into a concentrated CH_2Cl_2 solution. ^{1}H NMR (500 MHz, $CDCl_3$): 8.91 (d, 2H, J = 16.3 Hz), 7.83 (d, 2H, J = 16.2 Hz), 7.62 (d, 4H, J = 7.6 Hz), 7.49 (t, 3H, J = 6.2 Hz), 7.38−7.34 (m, 8H), 7.32−7.31 (m, 2H), 7.28 (d, 2H, J = 7.4 Hz), 7.09 (d, 4H, J = 8.0 Hz), 5.97 (s, 4H), 2.55 (s, 12H), 2.11−2.06 (m, 24H), 1.60−1.53 (m, 24H), 1.45 (d, 18H, J = 3.8 Hz), 1.36−1.29 (m, 24H), 0.82 (t, 36H, J = 14.6 Hz). ^{13}C NMR (100 MHz, $CDCl_3$): δ 155.2, 150.7, 143.2, 142.3, 140.7, 137.8, 137.5, 137.0, 136.0, 133.0, 131.5, 131.2, 130.9, 129.7, 128.9, 128.8, 128.7, 128.5, 128.4, 127.5, 121.1, 119.8, 118.9, 118.8, 118.7, 110.7, 110.6, 110.5, 109.4, 102.6, 29.7, 26.4, 24.4, 24.3, 24.3, 24.2, 24.1, 23.9, 14.6, 13.7, 12.7. MALDI-TOF-HRMS ($[C_{127}H_{169}B_3F_6N_6P_4Pt_2]^+$): calcd m/z = 2439.1838, found m/z = 2439.1865.

Synthesis of ***Pt−2****.*[43] **L−2** (35 mg, 0.10 mmol) and **1** (80 mg, 0.12 mmol) were dissolved in 8 mL of dried $NHEt_2$ under Ar. The mixture was stirred for 9 h at 45 °C. After the reaction was finished, the solvent was removed under reduced pressure. The residue was purified by column chromatography (silica gel, CH_2Cl_2/PE = 1:1, v/v). **Pt−2** was collected as a yellow solid (33 mg, 33.4%). ^{1}H NMR (500 MHz, $CDCl_3$): 7.33 (d, 2H, J = 8.2 Hz), 7.09 (d, 2H, J = 8.2 Hz), 5.97 (s, 2H), 2.55 (s, 6H), 2.06−2.01 (m, 12H), 1.63−1.55 (m, 12H), 1.48−1.41 (m, 18H), 0.92 (t, 18H, J = 7.3 Hz). MALDI-TOF-HRMS ($[C_{45}H_{72}BF_2N_2ClP_2Pt]^+$): calcd m/z = 981.4568, found m/z = 981.4573.

Nanosecond Transient Absorption Spectroscopy. Nanosecond transient absorption spectroscopy was studied with a LP920 laser flash photolysis spectrometer (Edinburgh Instruments, Livingston, U.K.). The samples were purged with N_2 for 15 min before measurements, and the N_2 gas flow was kept constant during the measurement. The signal was digitized with a Tektronix TDS 3012B oscilloscope.

Femtosecond Transient Absorption Spectroscopy. The ultrafast pump−probe transient absorption spectroscopy measurements were performed using a Ti:sapphire laser amplifier−optical parametric amplifier system (Spectra Physics, Spitfire Pro XP, TOPAS) and a commercial setup of ultrafast transient absorption spectrometer (Spectra Physics, Helios). Pulse duration was measured as 100 fs. Wavelengths of the pump beam were chosen according to the steady-state absorption spectra of the studied compounds. White light continuum generated with a sapphire crystal was used as a probe beam.

Cyclic Voltammetry. Cyclic voltammetry was performed under a 100 mV/s scan rate, in CHI610D Electrochemical workstation (Shanghai, China). The measurements were performed at room temperature with tetrabutylammonium hexafluorophosphate (Bu_4N-$[PF_6]$, 0.1 M) as the supporting electrolyte, glassy carbon electrode as the working electrode, and platinum electrode as the counter electrode. Dichloromethane was used as the solvent, and ferrocene (Fc) was added as the internal reference. The solution was purged with N_2 before measurement, and the N_2 gas flow was kept constant during the measurement.

The Gibbs Free Energy Changes (ΔG_{CS}) of the Photoinduced Electron Transfer. ΔG_{cs} was calculated with the Rehm−Weller equation.[72,73]

$$\Delta G_{CS} = e[E_{OX} - E_{RED}] - E_{00} + \Delta G_S \quad \text{(eq 1)}$$

$$\Delta G_S = -\frac{e^2}{4\pi\varepsilon_S\varepsilon_0 R_{CC}} - \frac{e^2}{8\pi\varepsilon_0}\left(\frac{1}{R_D} + \frac{1}{R_A}\right)\left(\frac{1}{\varepsilon_{REF}} - \frac{1}{\varepsilon_S}\right) \quad \text{(eq 2)}$$

where ΔG_S is the static Coulombic energy, e is electronic charge, E_{OX} is half-wave potential for one-electron oxidation of the electron-donor unit, E_{RED} is half-wave potential for one-electron reduction of the electron-acceptor unit, and E_{00} is energy level for the singlet-excited state approximated with the fluorescence emission wavelength or for the T_1 state energy of styrylBodipy. ε_S is static dielectric constant of the solvent, R_{CC} is center-to-center separation distance determined by DFT optimization of the geometry, R_D is the radius of the electron donor determined by DFT optimization of the geometry, R_A is the radius of the electron acceptor determined by DFT optimization of the geometry, ε_{REF} is the static dielectric constant of the solvent used for the electrochemical studies, and ε_0 is the permittivity of free space. The solvents used in the calculation were toluene (ε_S = 2.4), DCM (ε_S = 9.1), and MeCN (ε_S = 37.5).

$$E_{CS} = e[E_{OX} - E_{RED}] + \Delta G_S \quad \text{(eq 3)}$$

$$\Delta G_{CR} = -(\Delta G_{CS} + E_{00}) \quad \text{(eq 4)}$$

The energy transfer rate constant was calculated with eq 5.

$$k_{EnT} = \left[\frac{\Phi_{PL}(\text{Bodipy})}{\Phi_{PL}} - 1\right]/\tau(\text{Bodipy}) \quad \text{(eq 5)}$$

where $[\Phi_{PL}(\text{Bodipy})/\Phi_{PL}]$ is the fluorescence quantum yield ratio of the Bodipy unit in **Pt−2** and **Pt−1**, and τ(Bodipy) is the S_1 state lifetime of **Pt−2** (Table 2).

The triplet-state intermolecular energy-transfer rate constant was calculated with eq 6. The triplet-state energy-transfer efficiency was calculated with eq 7.

$$k_{ET} = (1/\tau_2) - (1/\tau_1) \quad \text{(eq 6)}$$

$$\Phi_{ET} = 1 - \tau_2/\tau_1 \quad \text{(eq 7)}$$

where τ_1 and τ_2 are triplet-state lifetime of the rising stage and decline stage of decay curves, respectively (Figure 11 and Supporting Information Figure S28).

The bimolecular quenching constant was calculated according to eq 8.

$$k_q = K_{SV}/\tau_0 \quad \text{(eq 8)}$$

where τ_0 is the triplet-state lifetime of the triplet-energy donor.

Quenching efficiency was given by eq 9, where k_0 is the diffusion-controlled bimolecular quenching rating constants, which can be calculated with the Smoluchowski eq 10.[89]

$$f_Q = k_q/k_0 \quad \text{(eq 9)}$$

$$k_0 = 4\pi RND/1000 = \frac{4\pi N}{1000}(R_f + R_q)(D_f + D_q) \quad \text{(eq 10)}$$

where D is the sum of the diffusion coefficients of the energy donor (D_f) and quencher (D_q), and N is Avogadro's number. R is the collision radius, the sum of the molecular radii of the energy donor (R_f) and the quencher (R_q).

DOI: 10.1021/acs.inorgchem.5b01107
Inorg. Chem. 2015, 54, 7492−7505

Diffusion coefficients can be obtained from Stokes−Einstein equation:[89]

$$D = kT/6\pi\eta R \quad \text{(eq 11)}$$

where k is Boltzmann's constant, η is the solvent viscosity, and R is the molecule radius.

Density Functional Theory Calculations. Geometry optimization was calculated by using the B3LYP functional, the vertical excitation energy was calculated with the TDDFT method based on the singlet ground-state geometry. All the calculations were performed with Gaussian 09W software (Gaussian, Inc.).[91]

Single-Crystal X-ray Diffractions. The crystal was mounted on glass fibers for X-ray measurement. Reflection data were collected at RT on a Bruker AXS SMART APEX II CCD diffractometer with graphite-monochromatized Mo Kα radiation (λ = 0.710 73 Å) and an ω scan mode. All the measured independent reflections ($I > 2\sigma(I)$) were used in the structural analyses, and semiempirical absorption corrections were applied using SADABS program. The structures were solved by the direct method using SHELXL-97. The hydrogen atoms of the organic frameworks were fixed at calculated positions geometrically and refined by using a riding model. In particular, the atoms on the phosphine ligand are found to be disordered and modeled over two split positions. All corresponding non-hydrogen atoms were refined by using the "Sadi" and "Simu" restraints to make the parameters of the disordered atoms more reasonable. CCDC No. (**Pt−0**): 1054164; CCDC No. (**Pt−1**): 1054152.

■ ASSOCIATED CONTENT

Supporting Information

^{1}H NMR and ^{13}C NMR data, selected bond lengths and angles, HRMS and photophysical spectra, and DFT/TDDFT calculation of the complexes. The Supporting Information is available free of charge on the ACS Publications website at DOI: 10.1021/acs.inorgchem.5b01107.

■ AUTHOR INFORMATION

Corresponding Authors

*E-mail: zhaojzh@dlut.edu.cn. (J.-Z.Z.)
*E-mail: xingyongheng2000@163.com. (Y.-H.X.)
*E-mail: hayvali@science.ankara.edu.tr. (M.H.)

Notes

The authors declare no competing financial interest.

■ ACKNOWLEDGMENTS

We thank the NSFC (20972024, 21273028, 21421005, and 21473020), Ministry of Education (SRFDP−-20120041130005), Program for Changjiang Scholars and Innovative Research Team in University [IRT_13R06], the Fundamental Research Funds for the Central Universities (DUT14ZD226), and Dalian University of Technology (DUT-2013TB07) for financial support.

■ REFERENCES

(1) Williams, J. A. G. *Top. Curr. Chem.* **2007**, *281*, 205−268.
(2) Feng, K.; Zhang, R.-Y.; Wu, L.-Z.; Tu, B.; Peng, M.-L.; Zhang, L.-P.; Zhao, D.; Tung, C.-H. *J. Am. Chem. Soc.* **2006**, *128*, 14685−14690.
(3) Kamegawa, T.; Matsuura, S.; Seto, H.; Yamashita, H. *Angew. Chem., Int. Ed.* **2013**, *52*, 916−919.
(4) Wang, W.-G.; Wang, F.; Wang, H.-Y.; Tung, C.-H.; Wu, L.-Z. *Dalton Trans.* **2012**, *41*, 2420−2426.
(5) (a) Mori, K.; Watanabe, K.; Fuku, K.; Yamashita, H. *Chem. - Eur. J.* **2012**, *18*, 415−418. (b) DiSalle, B. F.; Bernhard, S. *J. Am. Chem. Soc.* **2011**, *133*, 11819−11821.
(6) Shi, L.; Xia, W. *Chem. Soc. Rev.* **2012**, *41*, 7687−7697.
(7) Ravelli, D.; Fagnoni, M.; Albini, A. *Chem. Soc. Rev.* **2013**, *42*, 97−113.
(8) (a) Zhao, Q.; Li, F.; Huang, C. *Chem. Soc. Rev.* **2010**, *39*, 3007−3030. (b) Fernández-Moreira, V.; Thorp-Greenwood, F. L.; Coogan, M. P. *Chem. Commun.* **2010**, *46*, 186−202.
(9) Feng, Y.; Cheng, J.; Zhou, L.; Zhou, X.; Xiang, H. *Analyst* **2012**, *137*, 4885−4901.
(10) (a) Lo, K. K.-W.; Choi, A. W.-T.; Law, W. H.-T. *Dalton Trans.* **2012**, *41*, 6021−6047. (b) Law, W. H.-T.; Lee, L. C.-C.; Louie, M.-W.; Liu, H.-W.; Ang, T. W.-H.; Lo, K. K.-W. *Inorg. Chem.* **2013**, *52*, 13029−13041. (c) Louie, M.-W.; Choi, A. W.-T.; Liu, H.-W.; Chan, B. T.-N.; Lo, K. K.-W. *Organometallics* **2012**, *31*, 5844−5855.
(11) Vezzu, D. A. K.; Deaton, J. C.; Jones, J. S.; Bartolotti, L.; Harris, C. F.; Marchetti, A. P.; Kondakova, M.; Pike, R. D.; Huo, S. *Inorg. Chem.* **2010**, *49*, 5107−5119.
(12) (a) Tang, W.-S.; Lu, X.-X.; Wong, K. M.-C.; Yam, V. W.-W. *J. Mater. Chem.* **2005**, *15*, 2714−2720. (b) Liu, Z.; He, W.; Guo, Z. *Chem. Soc. Rev.* **2013**, *42*, 1568−1600.
(13) (a) Boixel, J.; Guerchais, V.; Le Bozec, H.; Jacquemin, D.; Amar, A.; Boucekkine, A.; Colombo, A.; Dragonetti, C.; Marinotto, D.; Roberto, D.; Righetto, S.; De Angelis, R. *J. Am. Chem. Soc.* **2014**, *136*, 5367−5375. (b) Yin, B.; Niemeyer, F.; Williams, J. A. G.; Jiang, J.; Boucekkine, A.; Toupet, L.; Le Bozec, H.; Guerchais, V. *Inorg. Chem.* **2006**, *45*, 8584−8596. (c) Cui, B.-B.; Zhong, Y.-W.; Yao, J. *J. Am. Chem. Soc.* **2015**, *137*, 4058−4061. (d) Cui, B.-B.; Mao, Z.; Chen, Y.; Zhong, Y.-W.; Yu, G.; Zhan, C.; Yao, J. *Chem. Sci.* **2015**, *6*, 1308−1315. (e) Vantomme, G.; Jiang, S.; Lehn, J.-M. *J. Am. Chem. Soc.* **2014**, *136*, 9509−9518.
(14) Zou, T.; Lok, C.-N.; Fung, Y. M. E.; Che, C.-M. *Chem. Commun.* **2013**, *49*, 5423−5425.
(15) (a) Djurovich, P. I.; Murphy, D.; Thompson, M. E.; Hernandez, B.; Gao, R.; Hunt, P. L.; Selke, M. *Dalton Trans.* **2007**, 3763−3770. (b) Zhao, Y.; Liu, Y.; Xu, Q.; Barahman, M.; Bartusik, D.; Greer, A.; Lyons, A. M. *J. Phys. Chem. A* **2014**, *118*, 10364−10371.
(16) Singh-Rachford, T. N.; Castellano, F. N. *Coord. Chem. Rev.* **2010**, *254*, 2560−2573.
(17) Zhao, J.; Ji, S.; Guo, H. *RSC Adv.* **2011**, *1*, 937−950.
(18) Ceroni, P. *Chem. - Eur. J.* **2011**, *17*, 9560−9564.
(19) Zhao, J.; Wu, W.; Sun, J.; Guo, S. *Chem. Soc. Rev.* **2013**, *42*, 5323−5351.
(20) Liu, R.; Azenkeng, A.; Li, Y.; Sun, W. *Dalton Trans.* **2012**, *41*, 12353−12357.
(21) Soliman, A. M.; Abdelhameed, M.; Zysman-Colman, E.; Harvey, P. D. *Chem. Commun.* **2013**, *49*, 5544−5546.
(22) Kim, K.-Y.; Liu, S.; Köse, M. E.; Schanze, K. S. *Inorg. Chem.* **2006**, *45*, 2509−2519.
(23) Chan, C. K. M.; Tao, C.-H.; Tam, H.-L.; Zhu, N.; Yam, V. W.-W.; Cheah, K.-W. *Inorg. Chem.* **2009**, *48*, 2855−2864.
(24) Wilson, J. S.; Chawdhury, N.; Al-Mandhary, M. R. A.; Younus, M.; Khan, M. S.; Raithby, P. R.; Köhler, A.; Friend, R. H. *J. Am. Chem. Soc.* **2001**, *123*, 9412−9417.
(25) Liu, Y.; Jiang, S.; Glusac, K.; Powell, D. H.; Anderson, D. F.; Schanze, K. S. *J. Am. Chem. Soc.* **2002**, *124*, 12412−12413.
(26) Glusac, K.; Köse, M. E.; Jiang, H.; Schanze, K. S. *J. Phys. Chem. B* **2007**, *111*, 929−940.
(27) Li, Y.; Köse, M. E.; Schanze, K. S. *J. Phys. Chem. B* **2013**, *117*, 9025−9033.
(28) Wu, W.; Zhao, J.; Sun, J.; Huang, L.; Yi, X. *J. Mater. Chem. C* **2013**, *1*, 705−716.
(29) Wu, W.; Zhao, J.; Guo, H.; Sun, J.; Ji, S.; Wang, Z. *Chem. - Eur. J.* **2012**, *18*, 1961−1968.
(30) Liu, L.; Guo, S.; Ma, J.; Xu, K.; Zhao, J.; Zhang, T. *Chem. - Eur. J.* **2014**, *20*, 14282−14295.
(31) Wu, W.; Wu, W.; Ji, S.; Guo, H.; Song, P.; Han, K.; Chi, L.; Shao, J.; Zhao, J. *J. Mater. Chem.* **2010**, *20*, 9775−9786.
(32) Wu, W.; Guo, H.; Wu, W.; Ji, S.; Zhao, J. *Inorg. Chem.* **2011**, *50*, 11446−11460.
(33) Liu, Y.; Wu, W.; Zhao, J.; Zhang, X.; Guo, H. *Dalton Trans.* **2011**, *40*, 9085−9089.
(34) Wu, W.; Ji, S.; Wu, W.; Shao, J.; Guo, H.; James, T. D.; Zhao, J. *Chem. - Eur. J.* **2012**, *18*, 4953−4964.

DOI: 10.1021/acs.inorgchem.5b01107
Inorg. Chem. 2015, 54, 7492−7505

(35) Wu, W.; Sun, J.; Cui, X.; Zhao, J. *J. Mater. Chem. C* **2013**, *1*, 4577−4589.
(36) Sun, J.; Wu, W.; Guo, H.; Zhao, J. *Eur. J. Inorg. Chem.* **2011**, *2011*, 3165−3173.
(37) Sun, J.; Wu, W.; Zhao, J. *Chem. - Eur. J.* **2012**, *18*, 8100−8112.
(38) Sun, J.; Zhong, F.; Yi, X.; Zhao, J. *Inorg. Chem.* **2013**, *52*, 6299−6310.
(39) Sun, J.; Zhong, F.; Zhao, J. *Dalton Trans.* **2013**, *42*, 9595−9605.
(40) Yi, X.; Zhao, J.; Wu, W.; Huang, D.; Ji, S.; Sun, J. *Dalton Trans.* **2012**, *41*, 8931−8940.
(41) Yi, X.; Zhang, C.; Guo, S.; Ma, J.; Zhao, J. *Dalton Trans.* **2014**, *43*, 1672−1683.
(42) Zhao, J.; Ji, S.; Wu, W.; Wu, W.; Guo, H.; Sun, J.; Sun, H.; Liu, Y.; Li, Q.; Huang, L. *RSC Adv.* **2012**, *2*, 1712−1728.
(43) Jia, H.; Küçüköz, B.; Xing, Y.; Majumdar, P.; Zhang, C.; Karatay, A.; Yaglioglu, G.; Elmali, A.; Zhao, J.; Hayvali, M. *J. Mater. Chem. C* **2014**, *2*, 9720−9736.
(44) Kozhevnikov, D. N.; Kozhevnikov, V. N.; Shafikov, M. Z.; Prokhorov, A. M.; Bruce, D. W.; Williams, J. A. G. *Inorg. Chem.* **2011**, *50*, 3804−3815.
(45) Liu, Y.; Guo, H.; Zhao, J. *Chem. Commun.* **2011**, *47*, 11471−11473.
(46) Ulrich, G.; Ziessel, R.; Harriman, A. *Angew. Chem., Int. Ed.* **2008**, *47*, 1184−1201.
(47) Benniston, A. C.; Copley, G. *Phys. Chem. Chem. Phys.* **2009**, *11*, 4124−4131.
(48) Lin, W.; Yuan, L.; Cao, Z.; Feng, Y.; Song, J. *Angew. Chem., Int. Ed.* **2010**, *49*, 375−379.
(49) Awuah, S. G.; You, Y. *RSC Adv.* **2012**, *2*, 11169−11183.
(50) Ziessel, R.; Harriman, A. *Chem. Commun.* **2011**, *47*, 611−631.
(51) Bozdemir, O. A.; Erbas-Cakmak, S.; Ekiz, O. O.; Dana, A.; Akkaya, E. U. *Angew. Chem., Int. Ed.* **2011**, *50*, 10907−10912.
(52) Coskun, A.; Akkaya, E. U. *J. Am. Chem. Soc.* **2005**, *127*, 10464−10465.
(53) Chan, C. K. M.; Tao, C.; Li, K.; Wong, K. M.-C.; Zhu, N.; Cheah, K.-W.; Yam, V. W.-W. *Dalton Trans.* **2011**, *40*, 10670−10685.
(54) Rogers, J. E.; Slagle, J. E.; Krein, D. M.; Burke, A. R.; Hall, B. C.; Fratini, A.; McLean, D. G.; Fleitz, P. A.; Cooper, T. M.; Drobizhev, M.; Makarov, N. S.; Rebane, A.; Kim, K.; Farley, R.; Schanze, K. S. *Inorg. Chem.* **2007**, *46*, 6483−6494.
(55) Wong, W.-Y.; Ho, C.-L. *Coord. Chem. Rev.* **2006**, *250*, 2627−2690.
(56) Zhong, F.; Karatay, A.; Zhao, L.; Zhao, J.; He, C.; Zhang, C.; Yaglioglu, H. G.; Elmali, A.; Küçüköz, B.; Hayvali, M. *Inorg. Chem.* **2015**; IC-2015-008822a, in press.
(57) Schanze, K. S.; Silverman, E. E.; Zhao, X. *J. Phys. Chem. B* **2005**, *109*, 18451−18459.
(58) Wu, W.; Guo, H.; Wu, W.; Ji, S.; Zhao, J. *J. Org. Chem.* **2011**, *76*, 7056−7064.
(59) Zhou, G.; Wong, W.-Y.; Poon, S.-Y.; Ye, C.; Lin, Z. *Adv. Funct. Mater.* **2009**, *19*, 531−544.
(60) Lu, J.-s.; Fu, H.; Zhang, Y.; Jakubek, Z. J.; Tao, Y.; Wang, S. *Angew. Chem., Int. Ed.* **2011**, *50*, 11658−11662.
(61) Dai, F.-R.; Zhan, H.-M.; Liu, Q.; Fu, Y.-Y.; Li, J.-H.; Wang, Q.-W.; Xie, Z.; Wang, L.; Yan, F.; Wong, W.-Y. *Chem. - Eur. J.* **2012**, *18*, 1502−1511.
(62) Eryazici, I.; Moorefield, C. N.; Newkome, G. R. *Chem. Rev.* **2008**, *108*, 1834−1895.
(63) Wong, W.-Y.; Harvey, P. D. *Macromol. Rapid Commun.* **2010**, *31*, 671−713.
(64) Castellano, F. N.; Pomestchenko, I. E.; Shikhova, E.; Hua, F.; Muro, M. L.; Rajapakse, N. *Coord. Chem. Rev.* **2006**, *250*, 1819−1828.
(65) Loudet, A.; Burgess, K. *Chem. Rev.* **2007**, *107*, 4891−4932.
(66) Harriman, A.; Mallon, L. J.; Elliot, K. J.; Haefele, A.; Ulrich, G.; Ziessel, R. *J. Am. Chem. Soc.* **2009**, *131*, 13375−13386.
(67) Chen, Y.; Zhao, J.; Guo, H.; Xie, L. *J. Org. Chem.* **2012**, *77*, 2192−2206.
(68) Valeur, B. *Molecular Fluorescence: Principles and Applications;* Wiley-VCH: Weinheim, Germany, 2001.
(69) Liu, J.-Y.; Huang, Y.; Menting, R.; Röder, B.; Ermilov, E. A.; Ng, D. K. P. *Chem. Commun.* **2013**, *49*, 2998−3000.
(70) El-Khouly, M. E.; Amin, A. N.; Zandler, M. E.; Fukuzumi, S.; D'Souza, F. *Chem. - Eur. J.* **2012**, *18*, 5239−5247.
(71) Poddutoori, P. K.; Zarrabi, N.; Moiseev, A. G.; Gumbau-Brisa, R.; Vassiliev, S.; van der Est, A. *Chem. - Eur. J.* **2013**, *19*, 3148−3161.
(72) Bura, T.; Nastasi, F.; Puntoriero, F.; Campagna, S.; Ziessel, R. *Chem. - Eur. J.* **2013**, *19*, 8900−8912.
(73) Ziessel, R.; Allen, B. D.; Rewinska, D. B.; Harriman, A. *Chem. - Eur. J.* **2009**, *15*, 7382−7393.
(74) Apperloo, J. J.; Martineau, C.; van Hal, P. A.; Roncali, J.; Janssen, R. A. J. *J. Phys. Chem. A* **2002**, *106*, 21−31.
(75) Kostereli, Z.; Ozdemir, T.; Buyukcakir, O.; Akkaya, E. U. *Org. Lett.* **2012**, *14*, 3636−3639.
(76) Whited, M. T.; Djurovich, P. I.; Roberts, S. T.; Durrell, A. C.; Schlenker, C. W.; Bradforth, S. E.; Thompson, M. E. *J. Am. Chem. Soc.* **2011**, *133*, 88−96.
(77) Wan, C. W.; Burghart, A.; Chen, J.; Bergström, F.; Johansson, L. B. Å.; Wolford, M. F.; Kim, T. G.; Topp, M. R.; Hochstrasser, R. M.; Burgess, K. *Chem. - Eur. J.* **2003**, *9*, 4430−4441.
(78) Bandichhor, R.; Petrescu, A. D.; Vespa, A.; Kier, A. B.; Schroeder, F.; Burgess, K. *J. Am. Chem. Soc.* **2006**, *128*, 10688−10689.
(79) Zhao, Y.; Zhang, Y.; Lv, X.; Liu, Y.; Chen, M.; Wang, P.; Liu, J.; Guo, W. *J. Mater. Chem.* **2011**, *21*, 13168−13171.
(80) Fan, J.; Hu, M.; Zhan, P.; Peng, X. *Chem. Soc. Rev.* **2013**, *42*, 29−43.
(81) Zhang, X.; Xiao, Y.; Qian, X. *Org. Lett.* **2008**, *10*, 29−32.
(82) Rachford, A. A.; Ziessel, R.; Bura, T.; Retailleau, P.; Castellano, F. N. *Inorg. Chem.* **2010**, *49*, 3730−3736.
(83) Wu, W.; Zhao, J.; Sun, J.; Guo, S. *J. Org. Chem.* **2012**, *77*, 5305−5312.
(84) Huang, L.; Zhao, J.; Guo, S.; Zhang, C.; Ma, J. *J. Org. Chem.* **2013**, *78*, 5627−5637.
(85) Huang, L.; Yu, X.; Wu, W.; Zhao, J. *Org. Lett.* **2012**, *14*, 2594−2597.
(86) Guo, S.; Ma, L.; Zhao, J.; Küçüköz, B.; Karatay, A.; Hayvali, M.; Yaglioglu, H. G.; Elmali, A. *Chem. Sci.* **2014**, *5*, 489−500.
(87) El-Khouly, M. E.; Fukuzumi, S. *J. Porphyrins Phthalocyanines* **2011**, *15*, 111−117.
(88) Feng, K.; Yu, M. L.; Wang, S. M.; Wang, G. X.; Tung, C. H.; Wu, L. Z. *ChemPhysChem* **2013**, *14*, 198−203.
(89) Lackowicz, J. R. *Principles of Fluorescence Spectroscopy,* 2nd ed.; Kluwer Academic: New York, 1999.
(90) Guo, J.; Huang, Z.; Wang, T.; Zhang, L.; Shao, J.; Guo, F. *Lett. Org. Chem.* **2013**, *10*, 22−26.
(91) Frisch, M. J.; Trucks, G. W.; aaaaSchlege, H. B.; Scuseria, G. E.; Robb, M. A.; Cheeseman, J. R.; Scalman, i. G.; Barone, V.; Mennucci, B.; Petersson, G. A.; Nakatsuji, H.; Caricato, M.; Li, X.; Hratchian, H. P.; Izmaylov, A. F.; Bloino, J.; Zheng, G.; Sonnenberg, J. L.; Hada, M.; Ehara, M.; Toyota, K.; Fukuda, R.; Hasegawa, J.; Ishida, M.; Nakajima, T.; Honda, Y.; Kitao, O.; Nakai, H.; Vreven, T.; Montgomery, J. A., Jr.; Peralta, J. E.; Ogliaro, F.; Bearpark, M.; Heyd, J. J.; Brothers, E.; Kudin, K. N.; Staroverov, V. N.; Kobayashi, R.; Normand, J.; Raghavachari, K.; Rendell, A.; Burant, J. C.; Iyengar, S. S.; Tomasi, J.; Cossi, M.; Rega, N.; Millam, M. J.; Klene, M.; Knox, J. E.; Cross, J. B.; Bakken, V.; Adamo, C.; Jaramillo, J.; Gomperts, R.; Stratmann, R. E.; Yazyev, O.; Austin, A. J.; Cammi, R.; Pomelli, C.; Ochterski, J. W.; Martin, R. L.; Morokuma, K.; Zakrzewski, V. G.; Voth, G. A.; Salvador, P.; Dannenberg, J. J.; Dapprich, S.; Daniels, A. D.; Farkas, O.; Foresman, J. B.; Ortiz, J. V.; Cioslowski, J.; Fox, D. J. *Gaussian 09;* Gaussian, Inc.: Wallingford, CT, 2009.

DOI: 10.1021/acs.inorgchem.5b01107
Inorg. Chem. 2015, 54, 7492−7505